Journal of Molecular Spectroscopy 348 (2018) 87–102

Contents lists available at ScienceDirect

Journal of Molecular Spectroscopy

journal homepage: www.elsevier.com/locate/jms

# High resolution analysis of the FTIR spectra of trifluoroamine $NF_3$

I.B. Bolotova [a], O.N. Ulenikov [a,b], E.S. Bekhtereva [a,b], S. Albert [a,c], S. Bauerecker [a,d], H. Hollenstein [a], Ph. Lerch [c], M. Quack [a,*], T. Peter [e], G. Seyfang [a], A. Wokaun [f]

[a] Physical Chemistry, ETH Zürich, CH-8093 Zürich, Switzerland
[b] Tomsk Polytechnic University, General Physics Department, 634050 Tomsk, Russia
[c] Swiss Light Source, PSI Villigen, Switzerland
[d] Institute of Physical and Theoretical Chemistry, TU Braunschweig, D-38106 Braunschweig, Germany
[e] Institute of Atmospheric and Climate Science, ETH Zürich, Switzerland
[f] Energy Research Department, PSI Villigen, Switzerland

ARTICLE INFO

*Article history:*
Received 5 October 2017
In revised form 9 April 2018
Accepted 9 April 2018
Available online 23 April 2018

*Keywords:*
Trifluoroamine ($NF_3$)
Atmospheric trace gases
Greenhouse effect
High resolution infrared spectroscopy
Overtones
Combination bands rovibrational analysis

ABSTRACT

We report high resolution Fourier Transform Infrared (FTIR) spectra of nitrogen trifluoride (trifluoroamine, $NF_3$) measured with the Zürich Bruker prototype spectrometer (ZP 2001) and the SLS THz/FTIR setup (2009 prototype) in the range 20–3000 $cm^{-1}$ at temperatures between 80 and 120 K using a collisional cooling cell designed with White cell multipath reflection optics and at room temperature (296 K). Except in the far-infrared with instrument limited resolution ($\Delta\tilde{\nu}_{FWHM}$ = 0.0008 $cm^{-1}$) many of the spectra are nearly Doppler limited. Rovibrational transitions were assigned to 13 different vibrational bands and were used then in the fitting procedure. We re-investigated the bands $2\nu_4, \nu_1, \nu_2+\nu_4, \nu_1+\nu_4$, $2\nu_3$ and $\nu_1+\nu_3$, which had been studied before, and we have analyzed the $\nu_2+\nu_3$, $2\nu_1, \nu_1+\nu_2+\nu_4, \nu_1+\nu_2+\nu_3, \nu_2+2\nu_3, 3\nu_3, \nu_1+2\nu_3$ bands for the first time. All our analyses refer to the isotopomer $^{14}NF_3$.

© 2018 Elsevier Inc. All rights reserved.

## 1. Introduction

Trifluoroamine (Nitrogen trifluoride, $NF_3$, Fig. 1) has found interest as a prototype molecule and fluorinated 'heavy' partner of the prototypical ammonia molecule. Its microwave spectrum has been studied early on [1–9], with later extensions also to the far infrared spectra [10]. These early studies have provided structural parameters, the dipole moment as well as the quadrupole coupling constant for the $^{14}N$ nucleus. Theoretical studies have addressed the barrier to inversion, which is remarkably high, estimated to be around 352 kJ/mol (3.6 eV) corresponding to about 29,000 $cm^{-1}$ according to the recent calculations [11–14].

More recently, trifluoroamine has also found interest as an atmospheric pollutant and greenhouse gas, which arises from a number of technical and industrial uses. It has been recently included in the second Kyoto protocol for this reason [15–18]. Its 100 year Global Warming Potential ($GWP_{100}$ referred to $CO_2$ as standard) is estimated to be about 17,200 [15]. In this context, the infrared spectra of $NF_3$ are of primordial importance and have already been studied at low, intermediate and high resolution [10,19–37], including also some more recent studies of the rotational spectra. The force field has been the subject of repeated studies [19,38,6,39] and the infrared band strengths were reported in [21,40–42].

Because of the increasing importance of $NF_3$ as an atmospheric trace gas, we aim here at a comprehensive investigation of the high resolution infrared spectra of $NF_3$ from the far infrared to about 3000 $cm^{-1}$. In this framework we have reinvestigated 6 vibrational bands at high resolution, extending the corresponding data base and the resolution in the lower wavenumber ranges. In the higher wavenumber ranges 2000–3000 $cm^{-1}$ we present also results with first high resolution analyses of 7 vibrational bands.

$NF_3$ is a symmetric top molecule (Fig. 1) with two totally symmetric and two degenerate normal vibrations summarized in Table 1 with the highest fundamental at 1032 $cm^{-1}$ ($\nu_1$, $NF_3$ symmetric stretching) followed by the $NF_3$ degenerate stretching $\nu_3$ at 907 $cm^{-1}$, the totally symmetric umbrella mode $\nu_2$ and the degenerate bending $\nu_4$ (see Table 1). Due to numerous intense overtone and combination bands it presents also a very rich spectrum in the wavenumber range 1000–3000 $cm^{-1}$ as shown in the surveys of Figs. 2 and 3.

We shall, in particular provide substantial information on $\nu_1$ and the spectra in these higher wavenumber ranges, which include the 'atmospheric window' and further regions of importance for

* Corresponding author.
*E-mail address:* martin@quack.ch (M. Quack).

https://doi.org/10.1016/j.jms.2018.04.004
0022-2852/© 2018 Elsevier Inc. All rights reserved.

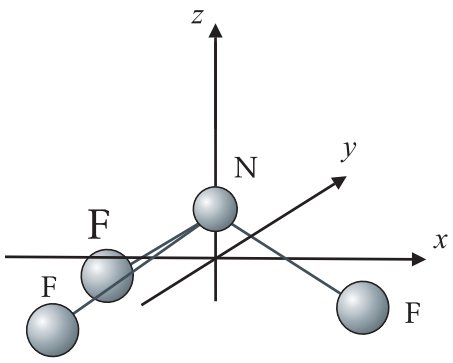


**Fig. 1.** Equilibrium structure and axes definition for $NF_3$.

the trace gas absorption. Some preliminary results were reported in [43] (see also [44]).

Infrared spectra of $NF_3$ were studied, *e.g.*, in [22–26,10,27,28]. More recently, a comprehensive investigation of the rovibrational spectrum of the molecule up to 2000 $cm^{-1}$ was reported in [29–37], which is also recently reviewed in [20]. In the present work we aim to accomplish an accurate analysis with new data and extend the knowledge about the high resolution FTIR spectra on $NF_3$ to the higher frequency range. The force field of $NF_3$ has been calculated by [38,5,6,39] and more recently by [19]. The intensities were studied by [40–42]. We have recalculated the molecular structure at the MP2/cc-pVDZ level [45,46] and our results agree well with a preceding systematic CCSD(T) study of the molecular structure [19] giving a best estimate for the NF bond length $r_e$ = 136.73 pm and the FNF angle $\alpha_e$ = 101.88 degrees. The harmonic vibrational wavenumbers $\omega_i$, the fundamentals $\nu_i$ and the infrared absorption intensities as measured and calculated for $NF_3$ are shown in Table 1. Being close in energy, the $\nu_1$ and $2\nu_4$ levels, as well as the levels of the $\nu_3$ mode, and their overtones form polyads. Nevertheless, many levels can be considered as isolated states in a first analysis.

In the present work we shall show the results of a systematic analysis of the Fourier-transform infrared spectra of $NF_3$ up to 3000 $cm^{-1}$. Some preliminary results were presented in [43]. Section 2 summarizes the experimental approach and conditions, Section 3 the theoretical model used in the analysis, Section 4 reports the far infrared spectra, Section 5 the spectra in the range 800–2000 $cm^{-1}$ and Section 6 the new analyses in the range 2000–3000 $cm^{-1}$.

## 2. Experimental

$NF_3$ was obtained from ABCR Chemicals with a stated purity of 99.99%. The identity of the substance, which was used without further purification but after degassing with freeze-pump thaw cycles, was obvious from the FTIR spectra.

We have measured the high resolution FTIR spectrum of $NF_3$ with the Bruker 125 HR Zürich Prototype spectrometer [47,48] in the spectral region 800–3000 $cm^{-1}$ and in the far infrared at the Swiss Light source with our Bruker IFS 125 (extended) prototype [49,50] (20–100 $cm^{-1}$). In order to record high resolution spectra in the region of 800–3000 $cm^{-1}$ (Fig. 3) we first measured spectra of collisionally cooled $NF_3$. The collisional cooling cell ([51,48]) is designed as a multipath White cell placed into a Dewar vessel filled with a coolant. Spectra were measured at a temperature of 80 K and a pressure $p$ = 0.02 mbar with a nominal resolution $\delta\tilde{\nu} = 1/d_{MOPD} = 0.001$ $cm^{-1}$ in the range 800–2000 $cm^{-1}$ and the temperature was then increased to 120 K [47,48] for the range 2000–3000 $cm^{-1}$. Further spectra were then measured at room temperature ($T$ = 296 K). The Doppler width is 0.00083 $cm^{-1}$ at 100 K and 1000 $cm^{-1}$ (0.0014 $cm^{-1}$ at 296 K), thus the spectra are generally about Doppler limited in the higher wavenumber ranges. In the far infrared the spectral resolution is instrument limited and Fig. 4 shows a detail of the far infrared (THz) spectrum. Table 2 summarizes the spectra measured here with details of the conditions. Pressure broadening is negligible in most of the spectra except (XI) with added $N_2$. While the natural isotope mixture was measured, all analyses refer to the isotopomer $^{14}NF_3$.

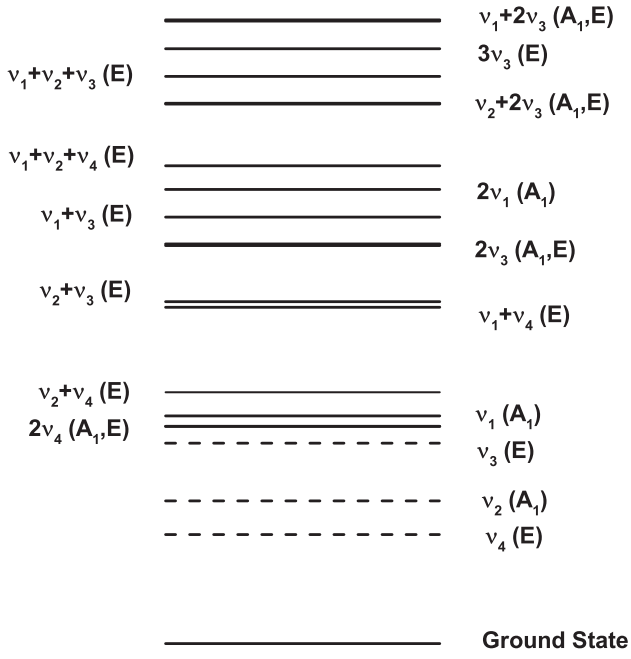


**Fig. 2.** Survey of energy levels of $NF_3$ as studied in this work.

## 3. Theoretical model

### 3.1. Symmetry considerations

Table 3 shows the character table for the point group $C_{3v}$ of $NF_3$. Similar to the case of $NH_3$, $NF_3$ in principle is non-rigid with the

**Table 1**
Calculated harmonic vibrational wavenumbers $\omega_i$ and fundamental vibrational wavenumbers $\nu_i$ compared to the experimental wavenumbers. Band intensities are as follows [21]: $A_1$ = 29.61 (46.5), $A_2$ = 1.54 (2.95), $A_3$ = 398 (201.4), and $A_4$ = 1.36 (0.46) all in km/mol with the theoretical values in the double harmonic approximation at the MP2 cc-pVDZ level in parenthesis [45].

| Method | | MP2 | CCSD(T) | Exp. | CCSD(T) | Exp. | |
|---|---|---|---|---|---|---|---|
| Basis set | | cc-pVDZ | aug-cc-pVQZ | | aug-cc-pVQZ | | |
| | | | $\omega_i$ | | $\nu_i$ | | |
| $i$ | Γ | [45] | [19] | this work | [19] | | Ref. |
| 1 | $A_1$ | 1043.9880 | 1053.8 | 1049.07 | 1035.5 | 1032.00 | this work |
| 2 | $A_1$ | 655.9070 | 660.7 | 654.40 | 648.7 | 647.13 | [20] |
| 3 | $E$ | 916.4460 | 935.7 | 929.77 | 912.7 | 907.54 | [20] |
| 4 | $E$ | 496.5823 | 502.8 | 500.57 | 494.0 | 493.42 | [20] |

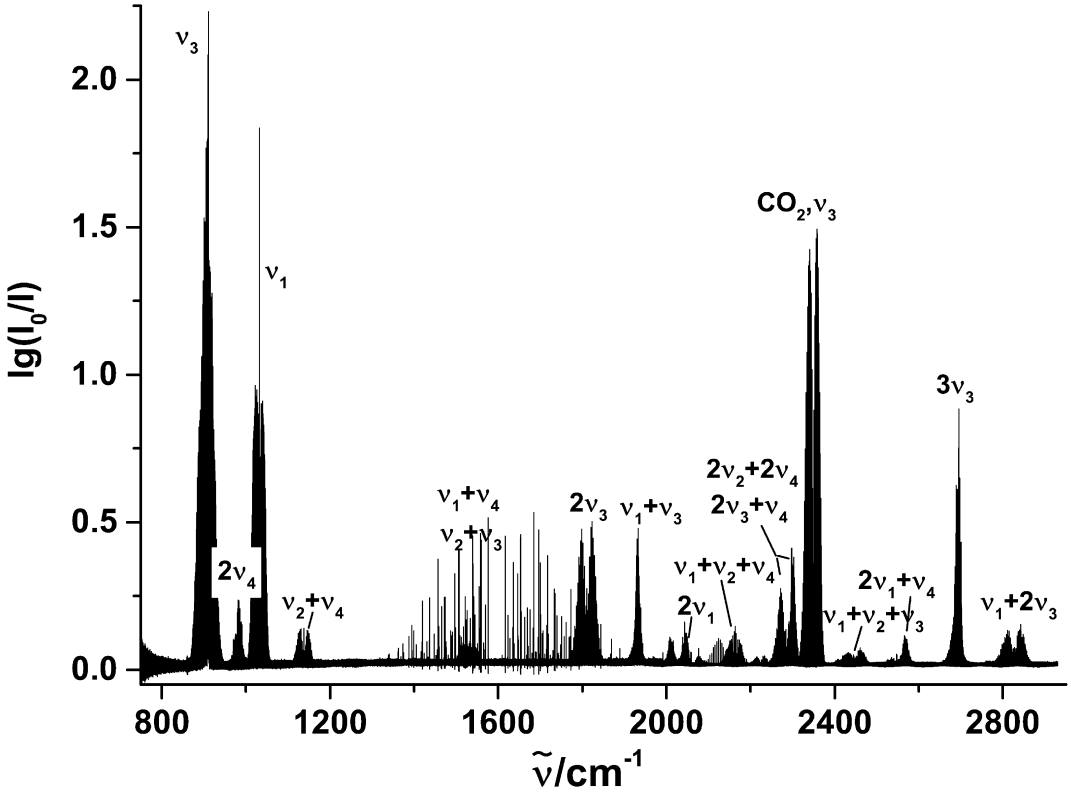


**Fig. 3.** Survey of the high resolution FTIR spectrum of $NF_3$ measured with the Zurich collisional cooling FTIR setup. The range 800–2000 $cm^{-1}$ was measured with resolution 0.001 $cm^{-1}$, path length $l$ = 7.5 m, pressure $p$ = 0.07 mbar at temperature T = 80 K; the 2000–3000 $cm^{-1}$ range was measured with a resolution 0.0033 $cm^{-1}$, $l$ = 7.5 m and $p$ = 1 mbar (with buffer gas He) at T = 120 K.

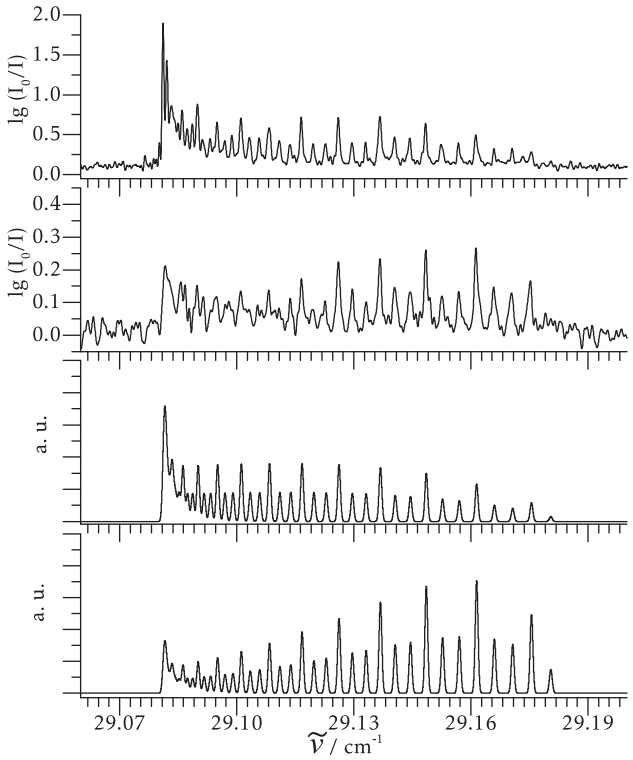


**Fig. 4.** High resolution far infrared spectrum of $NF_3$ measured at the Swiss Light Source at room temperature (top – $p$ = 2.2 mbar, $l$ = 10 m with the resolution 0.0008 $cm^{-1}$) and at T = 100 K using the collisional cooling cell (second line – $p$ = 3.5 mbar, $l$ = 10 m with the nominal resolution 0.0008 $cm^{-1}$). The third line is a simulation at T = 293 K and the fourth line at T = 100 K.

possibility of inversion, where the inversion sub levels can be classified according to the full permutation inversion group $S_3^*$, which for this case has as subgroup the molecular symmetry group $M_{S6}$ following Longuet-Higgins [52], isomorphous to $C_{3v}$, shown in Table 3 as well together with the induced representation $\Gamma_m \uparrow S_3^*$, the total nuclear spin $I(F_3)$ of the three F nuclei and the symmetry of the corresponding nuclear spin function. At the resolution of our experiments the inversion splittings are, however, not resolved, as the barrier in $NF_3$ is high and the effective tunneling mass is large.

Thus the case of $NF_3$ is more similar to $CHF_3$ [53,44,54,55] with respect to the tunneling substructure than to $NH_3$. Of course, different from $CHF_3$ there is no extra nuclear spin due to the H atom, but instead one has the nuclear spin of $^{14}N^{7+}$, which is a quadrupole nucleus with $I = 1$ and positive parity. As the fluorine nucleus with spin $I = 1/2$ has positive parity as well, the rovibronic parity gives at the same time the total parity. For further discussion of symmetry and nuclear hyperfine structure we refer to the recent discussion for $NH_3$ [56] and for the general background including the notation used here to [57,58].

In our experiments the nuclear hyperfine structure due to the $^{14}N$ nucleus is not resolved, but may contribute to the linewidth in some cases. The relative statistical weights 2:1 in the $K$ substructure follow from the same considerations as in [53] for $CHF_3$. Fig. 4 shows the high resolution spectrum in the THz (far infrared) range which shows nicely the expected patterns.

### 3.2. Effective Hamiltonian

The theoretical model for the effective Hamiltonian is essentially derived in symmetrized form in [59]. For the sake of convenience we briefly reproduce it here in order to provide the definitions of the parameters shown in the tables of the result

sections. In accordance with [59] the diagonal blocks, that are describing the rotational structure of an unperturbed vibrational state of $A_1$ – symmetry, can be written as a sum of the terms where H is given in wavenumber units (i.e. $H_{energy} = (hc)H$):

$$H^{A_1A_1}_{vib.-rot.} = H^{A_1A_1}_0 + H^{A_1A_1}_3 + H^{A_1A_1}_6 + \cdots, \quad (1)$$

where $H_0$, $H_3$, and $H_6$ are proportional to $J^0_\pm$, $J^3_\pm$ and $J^6_\pm$, respectively.

In particular, the first term can be expressed explicitly:

$$H^{A_1A_1}_0 = |A_1\rangle\langle A_1|\Big\{E^a + B^a(J^2_x + J^2_y) + C^aJ^2_z - D^a_JJ^4 - D^a_{JK}J^2J^2_z - D^a_KJ^4_z + H^a_JJ^6 + H^a_{JK}J^4J^2_z + H^a_{KJ}J^2J^4_z + H^a_KJ^6_z + L^a_JJ^8 + L^a_{JJK}J^6J^2_z + L^a_{JKK}J^4J^4_z + L^a_{JKK}J^2J^6_z + L^a_KJ^8_z \ldots\Big\}. \quad (2)$$

The second term in (1) is proportional to $J^3_\pm$ and can be written as follows:

$$H^{A_1A_1}_3 = |A_1\rangle\langle A_1|\Big\{\Big[\Big(\frac{1}{2}\epsilon^a + \frac{1}{2}\epsilon^a_JJ^2 + \epsilon^a_KJ^2_z\Big), \big(J^3_+ - J^3_-\big)\Big]_+ + \Big[\Big(\tilde{\epsilon}^aJ_z + \tilde{\epsilon}^a_JJ_zJ^2 + \tilde{\epsilon}^a_KJ^3_z\Big), \big(J^3_+ + J^3_-\big)\Big]_+\Big\}. \quad (3)$$

The third term in (1) is proportional to $J^6_\pm$ and can be written as follows:

$$H^{A_1A_1}_6 = |A_1\rangle\langle A_1|\Big[\Big(\frac{1}{2}\tilde{h}^a_3 + \frac{1}{2}\tilde{h}^a_3J^2 + \tilde{h}^a_{3K}J^2_z\Big), \big(J^6_+ - J^6_-\big)\Big]_+, \quad (4)$$

where $J_\pm = J_x \pm iJ_y$ $\left(i = \sqrt{-1}\right)$.

Eqs. (3) and (4) take into account the $a_1/a_2$ splittings for the $K = 3$ levels, that are typically observed in the spectra of the symmetric top molecules of $C_{3v}$ symmetry. It is known [60] that the $a_1/a_2$ splittings can be well described by the formula:

$$\Delta^J_3 = 2h_3J(J+1)[J(J+1) - 2][J(J+1) - 6], \quad (5)$$

where $h_3$ is the spectroscopic parameter, which describes the $a_1/a_2$ splitting.

One can show [61,62], that when:

$$\left|\frac{\tilde{\epsilon} < JK = 0|\left[\mathbf{J}_z, \left(\mathbf{J}^3_+ + \mathbf{J}^3_-\right)\right]|JK = \pm 3>}{9(C-B)}\right| \ll 1, \quad (6)$$

the $h_3$ parameter from (4) can be written as:

$$h_3 = \tilde{h}_3 - \frac{\tilde{\epsilon}^2}{C-B}. \quad (7)$$

This leads to the fact that the $\tilde{h}_3$ and $\tilde{\epsilon}$ parameters can not be determined separately and only their combination can be obtained from the experimental information. At the same time, the operator (5) takes into account the interactions between the states with $K \neq 3$ as the small corrections to the centrifugal distortion parameters in (2). This is not the case for the operator in Eq. (7), which mainly influences the $K = 3$ states. The experimental value for the $h_3$ parameter for the ground state of $NF_3$ molecule was found to be $h_3 = 1.777 \times 10^{13}$ cm$^{-1}$ [33]. Thereby the condition (6) is satisfied

**Table 2**
Overview of the high resolution spectra measured for $NF_3$.

| No. | $p$[a]/mbar | $T$[b]/K | $d$[c]/mm | $\delta\tilde{\nu}$[d]/cm$^{-1}$ | $l$[e]/m | Number of scans | Range/cm$^{-1}$ | Notes |
|---|---|---|---|---|---|---|---|---|
| I | 0.07 | 80 | 0.8 | 0.0010 | 7.5 | 200 | 800–4000 | [f] |
| II | 0.08 | 80 | 0.8 | 0.0010 | 7.5 | 214 | 800–4000 | [f] |
| III | 1 | 122 | 0.8 | 0.0033 | 7.5 | 424 | 2000–7000 | [g] |
| IV | 1 | 120 | 0.8 | 0.0033 | 7.5 | 280 | 1800–3500 | [h] |
| V | 1 | 296 | 1.0 | 0.0010 | 16 | 400 | 900–1300 | [i] |
| VI | 0.1 | 296 | 1.0 | 0.0010 | 3.2 | 336 | 900–1300 | [i] |
| VII | 1.0 | 296 | 1.0 | 0.0010 | 16.0 | 148 | 900–1300 | [i] |
| VIII | 0.2 | 296 | 0.8 | 0.0010 | 9.6 | 120 | 1050–2200 | [i] |
| IX | 6.9 | 296 | 0.8 | 0.0017 | 9.6 | 240 | 1800–3700 | [g] |
| X | 0.5 | 296 | 0.8 | 0.0017 | 3.2 | 100 | 1800–3600 | [g] |
| XI | 0.5 + 996($N_2$) | 296 | 0.8 | 0.005 | 3.2 | 790 | 1800–3600 | [g] |
| XII | 3.9 | 296 | 0.8 | 0.0017 | 19.2 | 400 | 1800–3700 | [g] |
| XIII | 0.05 | 296 | 0.8 | 0.0010 | 3.2 | 396 | 700–1450 | [g] |
| XIV | 1.0 | 296 | 1.0 | 0.0014 | 9.6 | 398 | 1100–1900 | [i] |
| XV | 2.2 | 296 | 3.15 | 0.0008 | 10.0 | 120 | 25–100 | [k] |
| XVI | 1.2 | 296 | 3.15 | 0.0008 | 10.0 | 120 | 25–100 | [k] |
| XVII | 3.5 | 100 | 3.15 | 0.0008 | 10.0 | 86 | 15–100 | [k] |
| XVIII | 0.7 | 296 | 0.8 | 0.0012 | 9.6 | 100 | 1500–2600 | [f] |
| XIX | 0.3 | 296 | 0.8 | 0.0012 | 9.6 | 100 | 1500–2600 | [f] |

[a] Pressure in the cell.
[b] Temperature.
[c] Diameter of entering circular aperture.
[d] Nominal resolution defined as $\delta\tilde{\nu} = 1/d_{MOPD}$ the actual instrumental resolution being better in general [47]. ($\Delta\tilde{\nu}_{FWHM} = 0.0006$ cm$^{-1}$ at 30 cm$^{-1}$ see also [53]).
[e] Absorbing path length $l$ in the (multireflection) cell.
[f] Source: Globar, Beamsplitter: KBr, Detector: MCT, Calibration gas: $H_2O$.
[g] Source: Tungsten, Beamsplitter: $CaF_2$, Detector: InSb, Calibration gas: $H_2O$.
[h] Source: Globar, Beamsplitter: KBr, Detector: InSb, Calibration gas: $H_2O$.
[i] Source: Globar, Beamsplitter: KBr, Detector: MCT, Calibration gas: OCS.
[k] Source: Synchrotron, Beamsplitter: Mylar 25$\mu$, Detector: Bolometer and cold filter, Calibration gas: $H_2O$.

**Table 3**
Character table for the $C_{3v}$ point group and the molecular symmetry group $M_{S6}$. $\Gamma_m \uparrow S^*_3$ is the induced representation in $S^*_3$ showing the sublevel structure. (Pauli forbidden species in $NF_3$ are set in parentheses), see [52,56–58,53]. $\Gamma_{ns}$ is the allowed nuclear spin function, the column $\mu$ gives the electric dipole moment components.

| | $C_{3v}$ | $E$ | $2C_3$ | $3\sigma_v$ | | $I_{(F_3)}$ | $\Gamma_{ns}$ | $\mu$ |
|---|---|---|---|---|---|---|---|---|
| $\Gamma_m$ | $M_{S6}$ | $E$ | 2(123) | 3(12)* | $\Gamma_m \uparrow S^*_3$ | | | |
| $A_1$ | | 1 | 1 | 1 | $(A^+_1) + A^-_2$ | 3/2 | $A^+_1$ | $\mu_z$ |
| $A_2$ | | 1 | 1 | −1 | $A^+_2 + (A^-_1)$ | 3/2 | $A^+_1$ | |
| $E$ | | 2 | −1 | 0 | $E^+ + E^-$ | 1/2 | $E^+$ | $\mu_x, \mu_y$ |

**Table 4**
Spectroscopic parameters of the vibrational ground state of $NF_3$ (in $cm^{-1}$).[a]

| Parameter | [27] | [19] | [32] | [33] | This work | 'Best' |
|---|---|---|---|---|---|---|
| 1 | 2 | 3 | 4 | 5 | 6 | 7 |
| $B$ | 0.3562838630(40) | 0.3562838630(66) | 0.3562827950 | 0.3562838556(21) | 0.3562821(109) | 0.3562838556 |
| $C$ | | | 0.19499250(44) | 0.19499250[b] | 0.19499250[b] | 0.19499250[b] |
| $D_J/10^{-6}$ | 0.4873648(60) | 0.4873531(36) | 0.4873517 | 0.48733446(273) | 0.4871(116) | 0.48733446 |
| $D_{JK}/10^{-6}$ | −0.759671(13) | −0.759645(16) | −0.759644 | −0.7596562(27) | −0.7597(179) | −0.7596562 |
| $D_K/10^{-6}$ | | | 0.34343(88) | | 0.34343[b] | 0.34343[b] |
| $H_J/10^{-12}$ | 0.65035(280) | 0.62760(8) | 0.6276 | 0.61352(106) | 0.5(40) | 0.61352 |
| $H_{JK}/10^{-11}$ | −0.3444(12) | −0.3335(33) | −0.3335 | −0.33510(33) | −0.34(81) | −0.33510 |
| $H_{KJ}/10^{-11}$ | 0.5027(25) | 0.4843(9) | 0.48433 | 0.48580(206) | 0.49(112) | 0.48580 |
| $H_K/10^{-11}$ | | | −0.10335(481) | | −0.10335[b] | −0.10335[b] |
| $L_J/10^{-18}$ | | 0.0 | | | | |
| $L_{JJK}/10^{-16}$ | | | | 0.380(36) | 0.380 | 0.380 |
| $L_{JK}/10^{-16}$ | | | | −0.964(103) | −0.964 | −0.964 |
| $L_{JKK}/10^{-16}$ | | | | 0.747(123) | 0.747 | 0.747 |
| $h_3/10^{-12}$ | | 0.1819(29) | | 0.1777(24) | 0.1777 | 0.1777 |
| $h_3^J/10^{-17}$ | | 0.68(14) | | −0.21(13) | −0.21 | −0.21 |
| $N_{tr}$ | | | 242 | 252 | 252 + 2024 | |
| $d_{rms}$ | | | 0.00032 | | 0.0004 | |

[a] Values in parentheses are standard uncertainties given as $1\sigma$ in units of the last digits quoted. If no uncertainties are given, the parameters were fixed in the fit as noted.
[b] Fixed to the value of column 4.

and both approaches using Eqs. (3) and (4) can be used equivalently to describe the $a_1/a_2$ splittings in the spectrum.

For the description of twofold degenerate vibrational states, one can write the Hamiltonian as the sum of terms proportional to different powers of the rotational operator:

$$H^{EE} = H_1^{EE} + H_2^{EE} + \cdots, \tag{8}$$

where individual terms are derived as (with $i = \sqrt{-1}$):

$$\begin{aligned} H_1^{EE} = {} & (|E_1\rangle\langle E_1| + |E_2\rangle\langle E_2|)\Big\{E^e + B^e(J_x^2 + J_y^2) + C^e J_z^2 - D_J^e J^4 - D_{JK}^e J^2 J_z^2 \\ & - D_K^e J_z^4 + H_J^e J^6 + H_{JK}^e J^4 J_z^2 + H_{KJ}^e J^2 J_z^4 + H_K^e J_z^6 + L_J^e J^8 + L_{JJK}^e J^6 J_z^2 + \ldots\Big\} \\ & + (|E_1\rangle\langle E_2| - |E_2\rangle\langle E_1|)\Big\{\eta^{vE} J_z + \eta_J J_z J^2 + \eta_K J_z^3 + \eta_{JJ} J_z J^4 + \eta_{JK} J_z^3 J^2 \\ & + \eta_{KK} J_z^5 + \eta_{JJJ} J_z J^6 + \eta_{JJK} J_z^3 J^4 + \eta_{JKK} J_z^5 J^2 + \eta_{KKK} J_z^7 + \ldots\Big\}, \end{aligned} \tag{9}$$

$$\begin{aligned} H_2^{EE} = {} & (|E_2\rangle\langle E_2| - |E_1\rangle\langle E_1|)\big\{[iA, (J_+ - J_-)]_+ + [B, (J_+ + J_-)]_+ \\ & + [C, (J_+^2 + J_-^2)]_+ + [iD, (J_-^2 - J_+^2)]_+\big\} \\ & + (|E_1\rangle\langle E_2| + |E_2\rangle\langle E_1|)\Big\{[A, (J_+ + J_-)]_+ + [iB, (J_- - J_+)]_+ \\ & + [iC, (J_+^2 - J_-^2)]_+ + [D, (J_+^2 + J_-^2)]_+\Big\}, \end{aligned} \tag{10}$$

where

$$\begin{aligned} A &= \frac{1}{2}\alpha + \frac{1}{2}\alpha_J J^2 + \alpha_K J_z^2 + \cdots, \\ B &= \beta J_z + \beta_J J_z J^2 + \beta_K J_z^3 + \cdots, \\ C &= \frac{1}{2}\gamma + \frac{1}{2}\gamma_J J^2 + \gamma_K J_z^2 + \cdots, \\ D &= \delta J_z + \delta_J J_z J^2 + \delta_K J_z^3 + \cdots. \end{aligned} \tag{11}$$

One can describe the interactions between vibrational states of different symmetry with the following off - diagonal matrix block:

$$\begin{aligned} H_{vib.-rot.}^{A_1E} = {} & |A_1\rangle\langle E_1|\Big\{[i\widetilde{A}, (J_+ - J_-)]_+ + [\widetilde{B}, (J_+ + J_-)]_+ + [\widetilde{C}, (J_+^2 + J_-^2)]_+ \\ & + [i\widetilde{D}, (J_-^2 - J_+^2)]_+\Big\} + |A_1\rangle\langle E_2|\Big\{[\widetilde{A}, (J_+ + J_-)]_+ \\ & + [i\widetilde{B}, (J_- - J_+)]_+ + [i\widetilde{C}, (J_+^2 - J_-^2)]_+ + [\widetilde{D}, (J_+^2 + J_-^2)]_+\Big\}. \end{aligned} \tag{12}$$

The operators $\{\widetilde{A}, \widetilde{B}, \widetilde{C}, \widetilde{D}\}$ can be expressed in the same manner, as before, with the set of coefficients $\{\tilde{\alpha}, \tilde{\beta}, \tilde{\gamma}, \tilde{\delta}\}$ (see also [63]).

## 4. Far infrared spectra and ground state parameters of $NF_3$

The vibrational ground state of the molecule was studied by microwave and far-infrared spectroscopy in [10,27,19]. The results are summarized in Table 4. The most recent study [33] (see column 5, Table 4) also provides the parameters of the $K = 3$ splitting obtained from the analysis of submillimeter-wave spectra. The $K$-dependent rotational and centrifugal distortion constants were obtained from the combination differences of transitions to the $2\nu_4$ ($E$) state by [32], see column 4 Table 4.

We have extended the spectroscopic information about the vibrational ground state of $NF_3$ substantially by measuring the rotational spectrum in the THz region using our ETH-SLS prototype setup combining the synchrotron source with the collisional cooling system. The spectra were recorded at room temperature, as well as at $T = 110$ K. As an illustration, an overview of the far-infrared spectrum is shown in the upper part of Fig. 5.

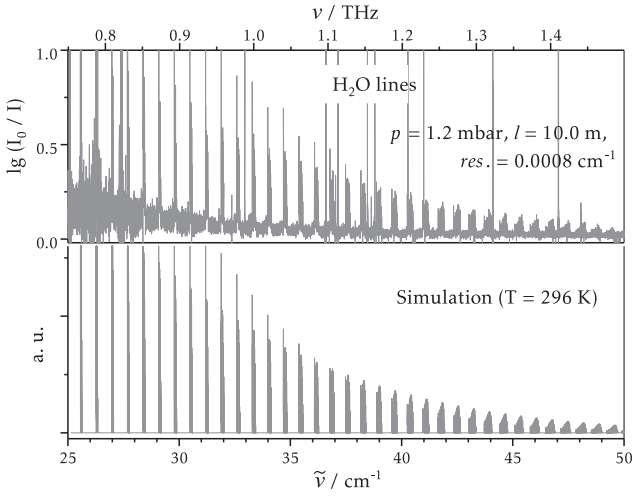


**Fig. 5.** Survey of the pure rotational spectrum of $NF_3$ measured in the far-infrared region ($p = 1.2$ mbar, $l = 10$ m) using our Bruker IFS 125 HR (extended) prototype spectrometer at the Swiss Light Source (upper trace) compared to the simulation based on the parameters from Table 4. Absorbance is shown as decadic logarithm, $\lg(I_0/I)$. (Spectrum XVI, the noise level increases below 30 $cm^{-1}$, see also Fig. 4.)

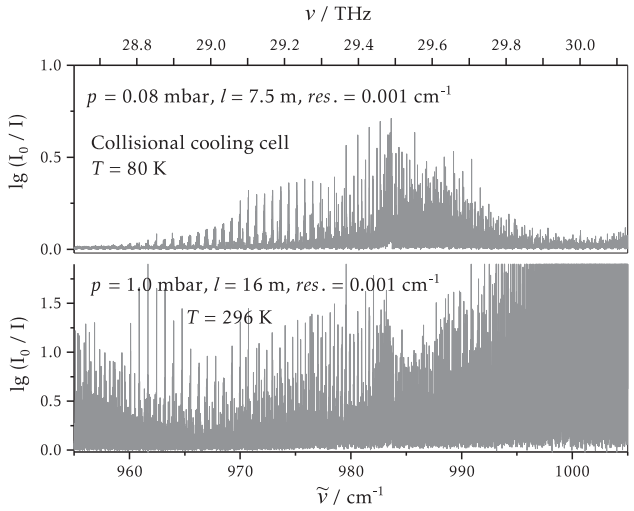


**Fig. 6.** Overview spectrum of the $2\nu_4$ band of $NF_3$ measured at room temperature ($T$ = 296 K; $p$ = 1 mbar, $l$ = 16 m) (bottom trace) and at $T$ = 80 K (top trace). $P$- and $R$-branches are clearly visible in the low temperature spectrum (top), whereas at room temperature the region is dominated by $R$−branch lines of the $\nu_3$ band and by $P$-branch lines of the $\nu_1$ fundamental (bottom). Absorbance is shown as decadic logarithm, $\lg(I_0/I)$. (Top: spectrum II, bottom: spectrum VII.)

More than 2000 rotational transitions up to $\tilde{\nu}_{max.} \approx 52.5\ cm^{-1}$, with maximum values of the rotational quantum numbers $J''_{max.}$ = 73 and $K''_{max.}$ = 69, were assigned. These data were combined with the transitions from [33] in a simultaneous fit, where submillimeter-wave and far-infrared data were weighted differently according to the accuracy of the corresponding experimental technique, giving the set of ground state parameters listed in column 6 of Table 4.

It should be noted that this substantial extension of the experimental data set leads to relatively large apparent fit uncertainties in the parameter values also, given the limitations of the model. Thus, for the analysis of the excited states of $NF_3$ discussed in the following sections of the present paper, we have used a combined set of parameters taking $J$-dependent values from column 5 of Table 4 and the $K$-dependent values were taken from column 4 of Table 4. The final 'best compromise' set of the spectroscopic parameters of the vibrational ground state of $NF_3$ is presented in column 7 of Table 4. A simulated rotational spectrum based on these parameters is shown in the bottom part of Fig. 5 and it agrees well with the experimental spectrum.

## 5. Re-analysis of spectra in the 800–2000 $cm^{-1}$ range

### 5.1. The $2\nu_4$ band

The $2\nu_4$ band of $NF_3$ is located around 985 $cm^{-1}$, see Fig. 6. It has two sub-band components from the corresponding levels, one of which is totally symmetric, $A_1$, the other one being degenerate, $E$. As one can see from Table 1 and from Fig. 3, the $2\nu_4$ level is close in energy to $\nu_3$ and $\nu_1$ and is situated between these two fundamentals. Being an overtone, it is also much less intense, which is why in the room temperature spectrum the $P$-branch is dominated by the $R$-branch of $\nu_3$, and its $R$-branch is mixed with rovibrational lines of the $\nu_1$ fundamental. This is shown in the lower part of Fig. 6, where the high resolution spectrum of the $2\nu_4$ overtone measured at $T$ = 296 K can be hardly recognised being hidden behind strong absorption lines of $\nu_3$ and $\nu_1$. In contrast, the upper part of Fig. 6 shows the low temperature ($T$ = 80 K) spectrum with an isolated band structure, which considerably simplifies the analysis. Despite the nearby fundamentals it is sufficient to consider $2\nu_4$ in an approximate isolated state model, as was also done in preceding studies [25,32] of these levels.

The spectra of $2\nu_4$ were studied first by [25] at modest resolution and also more recently by [32]. In the latter work the FTIR spectra were combined with the millimetre-wave data giving a set of parameters presented in Table 5 in columns 4 and 7 for two sub-levels of $2\nu_4$. Using this set of parameters we have started with an analysis of the low-temperature spectrum, where transi-

**Table 5**
Spectroscopic parameters of the $2\nu_4$ ($A_1$, $E$) vibrational overtone of $NF_3$ (in $cm^{-1}$).[a]

| Parameter | $2\nu_4(A_1)$ | $2\nu_4(A_1)$ | $2\nu_4(A_1)$ | $2\nu_4(E)$ | $2\nu_4(E)$ | $2\nu_4(E)$ |
|---|---|---|---|---|---|---|
| | This work 80 K | This work 296 K | [32] (Model 1) | This work 80 K | This work 296 K | [32] |
| 1 | 2 | 3 | 4 | 5 | 6 | 7 |
| $E^{a,e}$ | 983.7014268(132) | 983.7013913(258) | 983.701482(33) | 986.62299805(773) | 986.6226723(157) | 986.622336(18) |
| $\tilde{\nu}_0$[b] | | 983.70139(5) | | | 986.62267(2) | |
| $B$ | 0.35609737(16) | 0.356097296(157) | 0.35609070(21) | 0.355977564(82) | 0.355977913(83) | 0.355980556(41) |
| $C$ | 0.193888908(81) | 0.1938898393(56) | 0.19389053(17) | 0.193890515(62) | 0.193890601(35) | 0.19389176(11) |
| $D_J/10^{-6}$ | 0.509739(345) | 0.508623(187) | 0.51161(39) | 0.500979(154) | 0.502327(108) | 0.50142(16) |
| $D_{JK}/10^{-6}$ | −0.809662(536) | 0.808636(390) | −0.81165(83) | −0.793424(239) | −0.795831(227) | −0.79008(47) |
| $D_K/10^{-6}$ | 0.370629(255) | 0.372350(230) | 0.37340(56) | 0.362740(171) | 0.364241(130) | 0.35851(36) |
| $\eta^{vE}$[c] | | | | 0.6931239(6) | 0.6931208(8) | |
| $C\zeta$ | | | | | | −0.17327183(65) |
| $\eta_J/10^{-5}$ | | | | −0.27782(17) | −0.26748(12) | −0.18375(47) |
| $\eta_K/10^{-5}$ | | | | 0.23903(21) | 0.23119(13) | 0.16812(50) |
| $\eta_{JJ}/10^{-10}$ | | | | | | 0.582(48) |
| $\eta_{JK}/10^{-10}$ | | | | | | −3.952(52) |
| $\eta_{KK}/10^{-10}$ | | | | | | 3.241 |
| $\varepsilon/10^{-5}$ | | | | 0.92789(203) | 0.92245(786) | |
| $J_{max.}$ | | | | 30 | 55 | 42 |
| $K_{max.}$ | | | | 29 | 54 | 39 |
| $d_{rms}$ | (0.00007) | (0.00023) | | 0.00007 | 0.00023 | 0.00037 |

[a] Values in parentheses are 1$\sigma$ standard uncertainties. Parameters presented without uncertainties, as well as the sextic centrifugal distortion parameters $H_J$, $H_{JK}$, $H_{KJ}$ and $H_K$ were fixed to the corresponding values of the ground vibrational state Table 4.

[b] $\tilde{\nu}_0$ is the term value of the pure vibrational level ($J$ = 0).

[c] The parameter $\eta^{vE}$ can be related to the conventional $C\zeta$ by $\eta^{1E} = 2C\zeta$ for the fundamental and by $\eta^{2E} = -4C\zeta$ for the overtone, [63] (for the definition of $\varepsilon$ see also [53]. The number of data is 1341 at 80 and 2567 at 296 K, in Ref. [32] total 2747).

**Table 6**
Parameters of resonance interactions between the states $2\nu_4$ ($A_1$) and $2\nu_4$ ($E$) of $NF_3$ (in $cm^{-1}$)[a].

| Parameter | This work 80 K | This work 296 K | Parameter | [32] |
|---|---|---|---|---|
| $\tilde{\alpha}/10^{-2}$ | 0.17578(295) | 0.17663(141) | $q_4/10^{-2}$ | 0.170684(33) |
| $\tilde{\alpha}_J/10^{-6}$ | −0.128(10) | −0.149(39) | $q_J/10^{-8}$ | −0.551(43) |
| | | | $q_K/10^{-8}$ | 0.607(48) |
| $\tilde{\gamma}/10^{-3}$ | 0.854041(187) | 0.854466(908) | $r_4/10^{-3}$ | 0.17890(19) |
| $\tilde{\gamma}_J/10^{-8}$ | −0.110(87) | −0.1893(618) | $r_J/10^{-7}$ | −0.1280(49) |
| $\tilde{\gamma}_K/10^{-8}$ | | 0.1406(46) | $r_K/10^{-7}$ | 0.5507(80) |
| $\tilde{\kappa}/10^{-13}$ | | −0.568(14) | $F_{24}/10^{-6}$ | 0.236(23) |

[a] Values in parentheses are $1\sigma$ standard uncertainties. κ is defined by a contribution to the Hamiltonian as follows: $H_4 = (|E_2\rangle\langle E_2| - |E_1\rangle\langle E_1|)\left[F, \left(J_+^4 + J_-^4\right)\right]_+ + (|E_1\rangle\langle E_2| + |E_2\rangle\langle E_1|)\left[\mathrm{i}F, \left(J_+^4 - J_-^4\right)\right]_+$ with $F = \kappa/2+K$.

tions where assigned up to $J''_{max.} = 30$ and $K''_{max.} = 29$ being limited by the low temperature conditions. We then proceeded to the spectrum measured at the room temperature. The transitions with $J''_{max.} = 55$ and $K''_{max.} = 54$ were assigned, which extends the available spectroscopic data base for the rovibrational transitions in this band. Two fits were done independently for these spectra giving two sets of spectroscopic parameters presented in columns 2 and 5 of Table 5 for the low temperature ($T = 80$ K) data and in columns 3 and 6 for the room temperature transitions. The differences can be used for an estimate of systematic uncertainties in such fits. Of course, a combined fit of the data is possible as well. The interaction between $2\nu_4$ ($A_1$) and $2\nu_4$ ($E$) components was taken into account and the resonance interaction parameters are presented in Table 6. There is no direct correlation between the parameters from ref [32] and from the present work, being related to different Hamiltonians, although in principle a correlation could be established at least numerically. [32] gave several different parameter sets from different models, we present those from model 1 here.

### 5.2. The $\nu_1$ fundamental

The fundamental $\nu_1$ (symmetric $NF_3$-stretching) was studied by [26,27], where the high resolution FTIR data were combined with the transitions obtained by the saturation technique using $CO_2$ laser side bands as a tunable infrared source, where also the $K = 3$-splitting was observed. The resulting spectroscopic parameters are shown in Table 7 together with our new results.

**Table 7**
Spectroscopic parameters of the $\nu_1$ band of $NF_3$ (in $cm^{-1}$).[a]

| Parameter | This work 80 K | This work 296 K | [27] |
|---|---|---|---|
| 1 | 2 | 3 | 4 |
| $E^a$ | 1032.0014193(104) | 1032.001678(131) | 1032.00123750(47) |
| $\tilde{\nu}_0$[b] | 1032.0014193(104) | 1032.001678(131) | |
| $B$ | 0.35773176(548) | 0.35773265(501) | 0.3577335188(43) |
| $C$ | 0.194399205(737) | 0.194398394(887) | 0.1943989544(40) |
| $D_J/10^{-6}$ | 0.551987(591) | 0.555139(565) | 0.5549691(96) |
| $D_{JK}/10^{-6}$ | −0.92751(135) | −0.93646(138) | −0.935964(26) |
| $D_K/10^{-6}$ | 0.44599(109) | 0.44976(192) | 0.451706(30) |
| $H_J/10^{-11}$ | 0.06135 | 0.343(2) | 0.31971(57) |
| $H_{JK}/10^{-11}$ | −0.33509 | −1.6908(78) | −1.5624(25) |
| $H_{KJ}/10^{-11}$ | 0.4858 | 2.465(11) | 2.2729(43) |
| $H_K/10^{-11}$ | −0.10335 | −1.266(16) | −0.8970(26) |
| $J_{max.}$ | | 67 | 43(41) |
| $K_{max.}$ | | 49 | 41 |
| $N_{tr.}$ | | 3617 | 1295 + 158 |
| $d_{rms}$ | | 0.00010 | 0.0000018 |

[a] Values in parentheses are $1\sigma$ standard uncertainties. Parameters presented without uncertainties were fixed to the values of corresponding parameters of the ground vibrational state from Table 4.
[b] $\tilde{\nu}_0$ is the term value of the pure vibrational level ($J = 0$).

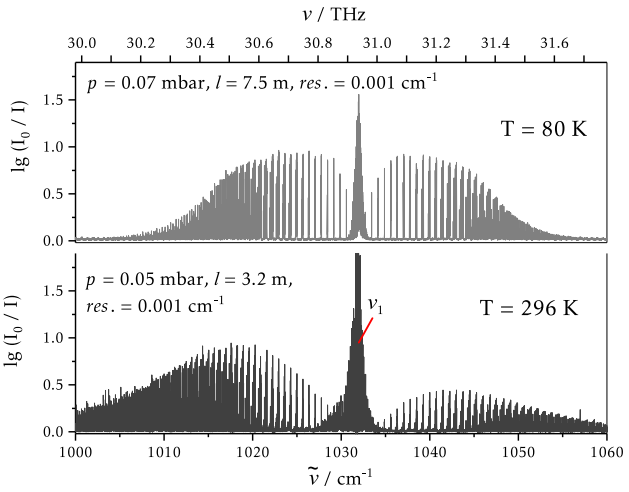


**Fig. 7.** Overview spectrum of the $\nu_1$ band of $NF_3$ measured at room temperature ($T = 296$ K) (bottom) and at $T = 80$ K (top). The spectrum shows a structure that is typical for a totally symmetric ($A_1$) band of $NF_3$, as expected for the $\nu_1$ fundamental. The lines with the same value of $J$ form clusters that are separated by $\approx 2B$ as can be seen in the Figure. Absorbance is shown as decadic logarithm, $\lg(I_0/I)$. (Top: spectrum I, bottom: spectrum XII.)

An overview of the $\nu_1$ spectra measured at room temperature and at $T = 80$ K is shown in Fig. 7. The spectrum shows a structure typical for the totally symmetric bands of $NF_3$ (due to the same molecular weight, rotational constants and $C_{3v}$ symmetry with three fluorine atoms this is also rather similar to the $^{12}CHF_3$ and $^{13}CHF_3$ spectra [53–55]). The assignment was therefore straightforward, giving more than 3500 rovibrational transitions with $J''_{max.} = 67$ and $K''_{max.} = 49$. Thereby, the spectroscopic database for the rovibrational transitions in the $\nu_1$ band of $NF_3$ was extended by about a factor of three compared to the data available in literature before.

The $\nu_1$ level can be perturbed by the close lying $\nu_3$ fundamental and by $2\nu_4$, but as it was already stated by [27] and was also seen in the present work, an approximate isolated state model is sufficient for the analysis. Similar to the previous case of the $2\nu_4$ level, the two sets of data obtained in two temperature regimes were fitted independently producing the sets of parameters presented in columns 2 and 3 of Table 7. Because of the larger data set, the room temperature results can be considered to be more reliable, agreeing well with the results of [27].

### 5.3. The $\nu_2 + \nu_4$ combination band

The $\nu_2 + \nu_4$ band was studied before by [64] and recently also at high resolution by [31]. The $\nu_2 + \nu_4$ band is located between 1080 and 1200 $cm^{-1}$. An overview spectrum measured with our Bruker 125 HR ZP2001 prototype spectrometer is shown in Fig. 8. Spectra

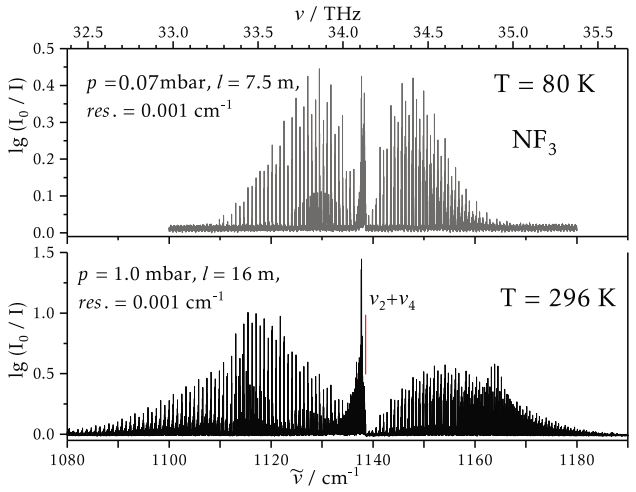


**Fig. 8.** Overview spectrum of the $\nu_2 + \nu_4$ band of $NF_3$ measured at room temperature ($T$ = 296 K; $p$ = 1 mbar, $l$ = 16 m) (bottom trace) and at $T$ = 80 K ($p$ = 0.07 mbar, $l$ = 7.5 m) (top trace). Absorbance is shown as decadic logarithm, lg($I_0/I$). (Top: spectrum I, bottom: spectrum VII.)

have been measured both at room temperature (296 K) and at low temperature (80 K). The nominal instrumental resolution defined as $1/d_{MOPD}$ (maximum optical path difference) was $\delta\tilde{\nu}$ = 0.001 cm$^{-1}$ for both spectra. The room temperature spectrum ($T$ = 296 K) was measured at $p$ = 1 mbar, $l$ = 16 m and aperture 1 mm using a Globar source, KBr beamsplitter and an MCT detector. The low temperature spectrum ($T$ = 80 K) was measured at $p$ = 0.07 mbar $l$ = 7.5 m and with an aperture of 0.8 mm. 280 scans have been co-added. As an illustration, a part of the high resolution spectra is shown in Fig. 9 for the $J'' = 8$ cluster of lines in the $R$-branch of $\nu_2 + \nu_4$. One can see that the low temperature spectrum is free of the "hot" band transitions.

The $\nu_2 + \nu_4$ band of nitrogen trifluoride has been carefully studied before in [31]. 4375 infrared and 119 MMW transitions where fitted together there yielding 22 parameters, which give the *rms*-deviation $d_{rms} = 0.27 \times 10^{-3}$ cm$^{-1}$ for the infrared transitions and $\sigma_{MMW}$ = 227 kHz for the microwave transitions. We, therefore, do not aim to considerably improve this accurate analysis, but rather to reproduce the data and to extend the database for rovibrational lines in this band. As a result of the high resolution analysis, about 4500 transitions were assigned to the $\nu_2 + \nu_4$ band with $J_{max.}$ = 80

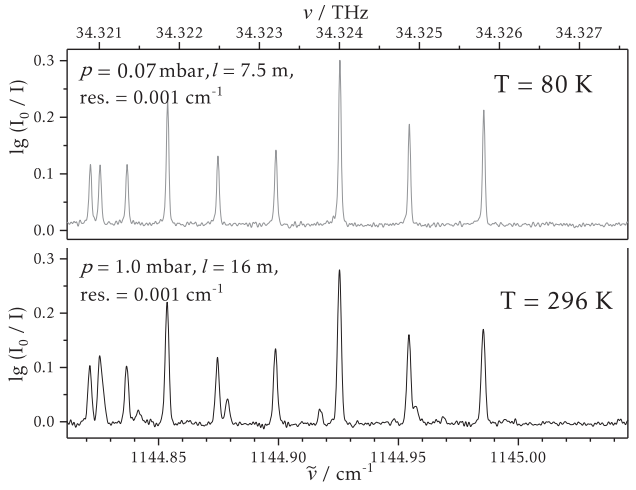


**Fig. 9.** Part of the high resolution spectrum of the $\nu_2 + \nu_4$ band of $NF_3$ for the cluster of lines $^{R}R_K(8)$. Absorbance is shown as decadic logarithm, lg($I_0/I$). (Top: spectrum I, bottom: spectrum VII.)

**Table 8**
Effective spectroscopic parameters of the $\nu_2 + \nu_4$ vibrational state of $NF_3$ (in cm$^{-1}$).[a]

| Parameter | This work $T$ = 80 K | This work $T$ = 296 K | [31] |
|---|---|---|---|
| 1 | 2 | 3 | 4 |
| $E^e$ | 1138.276645(13) | 1138.276625(91) | 1138.276649(15) |
| $\tilde{\nu}_0$[c] | 1138.2766 | 1138.2766 | 1138.2766 |
| $B$ | 0.354836434(113) | 0.35483563(4) | 0.354835485(68) |
| $C$ | 0.1940007916(757) | 0.193999979(18) | 0.194005878(39) |
| $D_J/10^{-6}$ | 0.490108(183) | 0.489189(47) | 0.488869(90) |
| $D_{JK}/10^{-6}$ | −0.764725(183) | −0.763814(99) | −0.76297(19) |
| $D_K/10^{-6}$ | 0.347190(215) | 0.345706(54) | 0.35369(10) |
| $H_J/10^{-11}$ | 0.06135 | 0.0625(16) | 0.1105(35) |
| $H_{JK}/10^{-11}$ | −0.33509 | −0.3344(51) | −0.552(11) |
| $H_{KJ}/10^{-11}$ | 0.4858 | 0.4774(57) | 0.819(12) |
| $H_K/10^{-11}$ | −0.10335 | −0.0977(21) | −0.3457(47) |
| $\eta^{\nu}E$ | −0.3477983(11) | −0.3477919(4) | |
| $C\zeta$ | | | −0.17389291(44) |
| $\eta_J/10^{-5}$ | 0.12536(34) | 0.12949(11) | 0.12810(20) |
| $\eta_K/10^{-5}$ | −0.11088(40) | −0.11646(11) | −0.11805(22) |
| $\eta_{JJ}/10^{-10}$ | | | 0.881(19) |
| $\eta_{JK}/10^{-10}$ | | | −1.672(38) |
| $\eta_{KK}/10^{-10}$ | | | 0.765(2) |
| $\varepsilon/10^{-3}$ | 0.422237(17) | 0.4233779(114) | 0.422798(7) x4 |
| $\varepsilon_J/10^{-8}$ | | −0.21755(92) | −0.0516(60) |
| $\varepsilon_K/10^{-8}$ | | 0.15572(94) | |
| $J_{max.}$ | 34 | 80 | 69(13)[b] |
| $K_{max.}$ | 34 | 77 | 69(13)[b] |
| $N_{tr.}$ | 1325 | 4450 | 4375(119)[b] |
| $d_{rms}$ | | 0.00015 | 0.00027(227 kHz)[b] |

[a] Values in parentheses are 1$\sigma$ standard errors. Parameters presented without uncertainties were fixed to the values of corresponding parameters of the vibrational ground state from Table 4

[b] Data obtained from the microwave transitions are shown in parentheses.

[c] $\tilde{\nu}_0$ is the term value of the pure vibrational level ($J$ = 0).

[d] The parameter $\eta^{\nu E}$ can be related to the conventional $C\zeta$ by $\eta^{1E} = 2C\zeta$ for the combination band with one quantum in the degenerate vibration, [63].

and $K_{max.}$ = 77, which exceeds the preceding data set for the rovibrational lines. On the basis of our analysis, the parameters of the effective Hamiltonian were obtained, which reproduce the experimental information with an accuracy close to the experimental uncertainties ($d_{rms}$ = 0.00015 cm$^{-1}$), see Table 8. As one

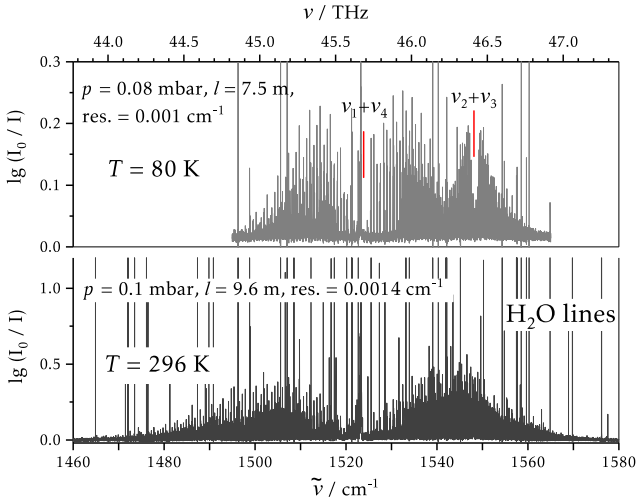


**Fig. 10.** Overview of the spectrum in the region of $\nu_1 + \nu_4$ and $\nu_2 + \nu_3$ bands of $NF_3$. The $\nu_2 + \nu_3$ band is directly seen in the low temperature spectrum ($T$ = 80 K, upper trace), whereas in the room temperature spectrum (bottom) its structure is hidden below the $R$-branch of the $\nu_1 + \nu_4$. Absorbance is shown as decadic logarithm, lg($I_0/I$). (Top: spectrum II, bottom: spectrum XIV).

can see, for the case of infrared transitions we could describe a larger set of spectroscopic data with a smaller set of parameters and slightly smaller $d_{rms}$. Small differences in the values of the high order spectroscopic parameters arise from the differences in the effective Hamiltonian models used in the different approaches.

### 5.4. The $\nu_1 + \nu_4$ and $\nu_2 + \nu_3$ bands

$\nu_1 + \nu_4$ is a perpendicular combination band located around 1520 cm$^{-1}$. An overview of the room temperature ($T$ = 296 K) spectrum is shown in the bottom part of Fig. 10. The band was studied by [35,36] where the $\nu_1 + \nu_4$ level of symmetry $E$ was considered in an isolated state model. Although a possible resonance interaction with $\nu_2 + \nu_3$ was pointed out before [35,36], it was not included in the fitting, because the rovibrational transitions in $\nu_2 + \nu_3$ could not be observed being covered by the $R$-branch lines of $\nu_1 + \nu_4$.

**Table 9**
Spectroscopic parameters of the $\nu_1 + \nu_4$ and $\nu_2 + \nu_3$ vibrational states of $NF_3$.[a]

| Parameter | $\nu_1 + \nu_4$ This work | $\nu_1 + \nu_4$ [35] | $\nu_2 + \nu_3$ This work |
|---|---|---|---|
| 1 | 2 | 3 | 4 |
| $E^e$ | 1523.3048611(260) | 1523.040783(34) | 1548.2717812(261) |
| $\tilde{\nu}_0$ | 1523.3048611(260) | 1523.040783(34) | 1548.2717812(261) |
| $B$ | 0.35746676(11) | 0.35741397(44) | 0.35240739(10) |
| $C$ | 0.193822266(80) | 0.19361911(40) | 0.193809767(75) |
| $D_J/10^{-6}$ | 0.552308(148) | 0.5834(16) | 0.446231(109) |
| $D_{JK}/10^{-6}$ | −0.924714(407) | −0.9693(33) | −0.652590(289) |
| $D_K/10^{-6}$ | 0.442880(303) | 0.6267(23) | 0.278079(220) |
| $H_J/10^{-11}$ | 0.06135 | 2.45(16) | 0.06135 |
| $H_{JK}/10^{-11}$ | −0.33509 | −24.39(43) | −0.33509 |
| $H_{KJ}/10^{-11}$ | 0.4858 | 7.25(48) | 0.4858 |
| $H_K/10^{-11}$ | −0.10335 | 8.66(34) | −0.10335 |
| $h_3/10^{-12}$ | 0.1777 | | 0.1777 |
| $h'_3/10^{-17}$ | −0.213 | | −0.213 |
| $\eta^{vE}$ | −0.3491829(15)[c] | | 0.3116456(15)[c] |
| $C\zeta$ | | −0.1705393(37) | |
| $\eta_J/10^{-5}$ | 0.15154(71) | −0.112(12) | −0.49431(74) |
| $\eta_K/10^{-5}$ | −0.1454(85) | −0.416(12) | 0.48551(73) |
| $\eta_{JJ}/10^{-10}$ | −0.168(29) | −0.01768(58) | 0.2064(25) |
| $\eta_{JK}/10^{-10}$ | 0.416(59) | 0.0261(11) | −0.4277(55) |
| $\eta_{KK}/10^{-10}$ | −0.226(30) | −0.01296(55) | 0.2220(30) |
| $\tau_{JJJ}/10^{-12}$ | | 0.1322(68) | |
| $\tau_{JJK}/10^{-12}$ | | −0.247(19) | |
| $\tau_{JKK}/10^{-11}$ | | 0.55(19) | |
| $\tau_{KKK}/10^{-11}$ | | 0.574(67) | |
| $\alpha/10^{-3}$ | 0.4582017(1) | | −0.989640(21) |
| $\alpha_J/10^{-8}$ | −0.4604(85) | | 2.333(21) |
| $\alpha_K/10^{-8}$ | 0.2659(14) | | 12.101(26) |
| $q/10^{-4}$ | | 0.173009(83) | |
| $q_J/10^{-8}$ | | 0.446(38) | |
| $q_{JJ}/10^{-11}$ | | −0.1125(43) | |
| $q_{JK}/10^{-12}$ | | −0.125(18) | |
| $r/10^{-6}$ | | ±0.129(93) | |
| $r_J/10^{-9}$ | | 0.0 | |
| $t/10^{-10}$ | | −0.849 | |
| $h_3/10^{-14}$ | | 0.228(74) | |
| $J_{max.}$ | 55 | 70 | 49 |
| $K_{max.}$ | 53 | 70 | 48 |
| $N_{tr.}$ | 1496 | 1885 | 1586 |
| $d_{rms}$ | | 0.000288 | 0.00020 |

[a] Values in parentheses are 1$\sigma$ standard uncertainties. Parameters presented without uncertainties were fixed to the values of the corresponding parameters of the vibrational ground state from Table 4.
[b] $\tilde{\nu}_0$ is the term value of the pure vibrational level ($J = 0$).
[c] The parameter $\eta^{vE}$ can be related to the conventional $C\zeta$ by $\eta^{1E} = 2C\zeta$ for the combination with one quantum in the degenerate vibration, [63].

The results obtained by [35] for $\nu_1 + \nu_4$ in an isolated state model analysis are shown in column 3 in Table 9.

Indeed, in the room temperature spectrum (bottom trace in Fig. 10) the $\nu_1 + \nu_4$ band is predominant and strong $H_2O$ absorption lines are located in this range, which were used for calibration. The spectrum appears quite different at low temperature ($T$ = 80 K, upper trace in Fig. 10). Both the $\nu_1 + \nu_4$ and $\nu_2 + \nu_3$ band structures can be recognised, which considerably simplifies the analysis. Our analysis of this spectrum gave about 1500 lines assigned for each band with $J_{max.}$ = 55 and $K_{max.}$ = 53 for the $\nu_1 + \nu_4$ and $J_{max.}$ = 49 and $K_{max.}$ = 48 for $\nu_2 + \nu_3$. Extending this analysis to the room temperature spectrum will give even more spectroscopic information about the transitions. The parameters of the effective Hamiltonian obtained are presented in columns 2 and 4 in Table 9 and the resonance interaction parameters are shown in Table 10. This set of parameters describes the experimental information with high accuracy ($d_{rms}$ = 0.0002 cm$^{-1}$, which is close to the experimental uncertainty). We note the different effective Hamiltonians as used here and in [35].

### 5.5. The $2\nu_3$ overtone

Fig. 11 shows an overview of the $2\nu_3$ ($A_1/E$) overtone spectrum measured at room temperature (middle and bottom) and at $T$ = 80 K (top). The band was studied before by [34] at high resolution ($\delta\tilde{\nu}$ = 0.0025 cm$^{-1}$) and the results of the analysis are shown in columns 2 and 3 in Table 11 and in column 2 in Table 12.

For the sake of completeness of our analysis we have reanalysed the $2\nu_3$ band at even higher resolution in the low temperature spectrum. The results of the analysis are shown in Tables 11 and 12. The low temperature spectrum provides fewer transitions with

**Table 10**
Parameters of the resonance interaction between the $\nu_1 + \nu_4$ and $\nu_2 + \nu_3$ vibrational states of $NF_3$ (in cm$^{-1}$)[a].

| Parameter | Value |
|---|---|
| 1 | 2 |
| $\alpha$ | 2.57979(12) |
| $\beta/10^{-2}$ | 0.5956(35) |
| $\gamma/10^{-4}$ | 0.2935(69) |

[a] Values in parentheses are 1$\sigma$ standard uncertainties.

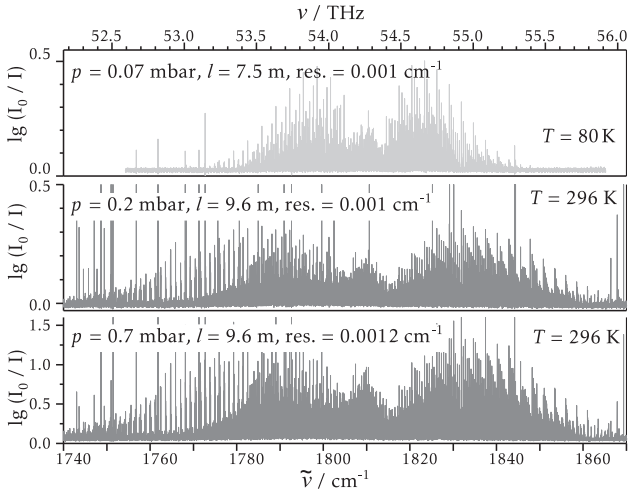


**Fig. 11.** Survey spectrum of the $2\nu_3$ band of $NF_3$ measured at room temperature ($T$ = 296 K) at two pressures (middle and bottom) and at $T$ = 80 K (top trace). The structure of the spectrum is considerably simplified in the low temperature measurements. Absorbance is shown as decadic logarithm, lg($I_0/I$). (Top: spectrum I, middle: spectrum VIII, bottom: spectrum XIV.)

**Table 11**
Spectroscopic parameters of the $2\nu_3$ ($A_1/E$) vibrational levels of $NF_3$ (in $cm^{-1}$).[a]

| Parameter | $2\nu_3$ ($A_1$) [34] | $2\nu_3$ ($E$) [34] | $2\nu_3$ ($A_1$) This work | $2\nu_3$ ($E$) This work |
|---|---|---|---|---|
| 1 | 2 | 3 | 4 | 5 |
| $E^{a,e}$ | | | 1803.130641(13) | 1810.424372(50) |
| $\tilde{\nu}_0$ | 1803.130221(56) | 1810.423992(21) | 1803.130641(13)[b] | 1810.424372(50)[b] |
| $B$ | 0.35143972(22) | 0.35103579(12) | 0.35143902(19) | 0.35103058(73) |
| $C$ | 0.19351716(36) | 0.193494871(68) | 0.19351745(11) | 0.19349565(35) |
| $D_J/10^{-6}$ | 0.42955(18) | 0.41900(20) | 0.41604(31) | 0.41980(52) |
| $D_{JK}/10^{-6}$ | −0.60835(53) | −0.57394(41) | −0.58763(67) | −0.57796(12) |
| $D_K/10^{-6}$ | 0.25430(57) | 0.22831(23) | 0.24849(44) | 0.23042(83) |
| $H_J/10^{-11}$ | | −0.24947(90) | 0.06135 | 0.06135 |
| $H_{JK}/10^{-11}$ | | 1.1436(29) | −0.33509 | −0.33509 |
| $H_{KJ}/10^{-11}$ | | −1.5212(32) | 0.4858 | 0.4858 |
| $H_K/10^{-11}$ | | 0.680(12) | −0.10335 | −0.10335 |
| $\eta^{vE}$ | | | | −0.6174301(43)[c] |
| $C\zeta$ | | 0.15436018(50) | | |
| $\eta_J/10^{-5}$ | | 0.69677(41) | | 1.2240(92) |
| $\eta_K/10^{-5}$ | | −0.68378(39) | | −1.1953(92) |
| $\eta_{JJ}/10^{-9}$ | | −0.4092(53) | | |
| $\eta_{JK}/10^{-9}$ | | 0.9417(100) | | |
| $\eta_{KK}/10^{-9}$ | | −0.5402(50) | | |
| $\tau_{JJJ}/10^{-13}$ | | 0.155(19) | | |
| $\tau_{JJK}/10^{-13}$ | | −0.661(58) | | |
| $\tau_{JKK}/10^{-13}$ | | 0.849(58) | | |
| $\tau_{KKK}/10^{-13}$ | | −0.300(20) | | |
| $\alpha$ | | | | −0.43481(36) |
| $J_{max.}$ | 43 | 69 | 32 | 40 |
| $K_{max.}$ | 30 | 65 | 24 | 40 |
| $N_{tr.}$ | | 3695 | 234 | 2031 |
| $d_{rms}$ | 0.00035 | | 0.00021 | |

[a] Values in parentheses are $1\sigma$ standard uncertainties. Parameters presented without uncertainties were fixed to the values of corresponding parameters of the vibrational ground state from Table 4.
[b] $\tilde{\nu}_0$ is the term value of the pure vibrational level ($J = 0$).
[c] The parameter $\eta^{vE}$ can be related to the conventional $C\zeta$ by $\eta^{1E} = 2C\zeta$ for the fundamental and by $\eta^{2E} = -4C\zeta$ for the overtone, [63].

**Table 12**
Interaction parameters between the $2\nu_3$ ($A_1$) and $2\nu_3$ ($E$) vibrational states of $NF_3$ (in $cm^{-1}$)[a].

| Parameter | [34] | Parameter | This work |
|---|---|---|---|
| 1 | 2 | 3 | 4 |
| $q/10^{-2}$ | −0.386795(14) | $\tilde{\alpha}/10^{-2}$ | 0.4147(28) |
| $q_J/10^{-7}$ | 0.5408(15) | $\tilde{\alpha}_J/10^{-6}$ | −0.306(44) |
| $q_{JJ}/10^{-11}$ | −0.2673 | $\tilde{\beta}/10^{-3}$ | 0.29846(53) |
| $r/10^{-3}$ | 0.187848 | $\tilde{\gamma}/10^{-2}$ | −0.19216(15) |
| $r_J/10^{-10}$ | 0.736(86) | | |
| $\varepsilon/10^{-7}$ | −0.558(11) | | |
| $f_{24}/10^{-4}$ | 0.102462(93) | | |
| $f_{44}/10^{-9}$ | −0.6578(77) | | |

[a] Values in parentheses are $1\sigma$ standard uncertainties.

lower rotational quantum numbers, about 2250 transitions were assigned for both bands with $J_{max.} = K_{max.} = 40$. Therefore, fewer spectroscopic parameters are needed to describe the spectrum at high accuracy ($d_{rms} = 0.00021\ cm^{-1}$). The analysis can be further substantially extended by adding the rovibrational transitions from the room temperature spectra (see Fig. 11) to the higher $J$ and $K$ values. In comparing values of parameters from previous work and our present analysis one must take into account the different definitions in the different effective Hamiltonians.

### 5.6. The $\nu_1 + \nu_3$ combination band

The $\nu_1 + \nu_3$ combination located around 1930 $cm^{-1}$ is very close to the $2\nu_3$ level, which was discussed in the previous section. Both bands were studied by [34] at high resolution and we only aim to reproduce the data at higher resolution for completeness in our systematic analysis.

An overview spectrum of $\nu_1 + \nu_3$ is shown in Fig. 12. The structure of the band is somewhat similar to the neighbouring $2\nu_3$ band. We have analysed the spectra measured at low temperature (top trace in Fig. 12), as well as the room temperature spectra (middle trace in Fig. 12), which gave us about 2800 rovibrational transitions with $J_{max.} = 63$, $K_{max.} = 45$ that were used in the fit. At a subsequent stage of the analysis this data set may be further extended to higher $J$ and $K$ values by considering the saturated spectrum shown at the bottom in Fig. 12. This will allow for the analysis of many further, weaker lines.

The results of the fit are presented in Table 13. 2800 lines were described with a relatively small set of spectroscopic parameters with $d_{rms} = 0.00037\ cm^{-1}$.

## 6. New analyses of the spectra in the 2000–3000 $cm^{-1}$ range

The structure of the high resolution spectra of $NF_3$ in the higher frequency and wavenumber ranges was not completely understood previously and in the present section we show our results for the newly measured and analyzed rovibrational bands of $NF_3$ from 2000 to 3000 $cm^{-1}$.

### 6.1. The $2\nu_1$ band around 2060 $cm^{-1}$

The $2\nu_1$ overtone band is a relatively weak band located around 2060 $cm^{-1}$. An overview spectrum of the band measured at room

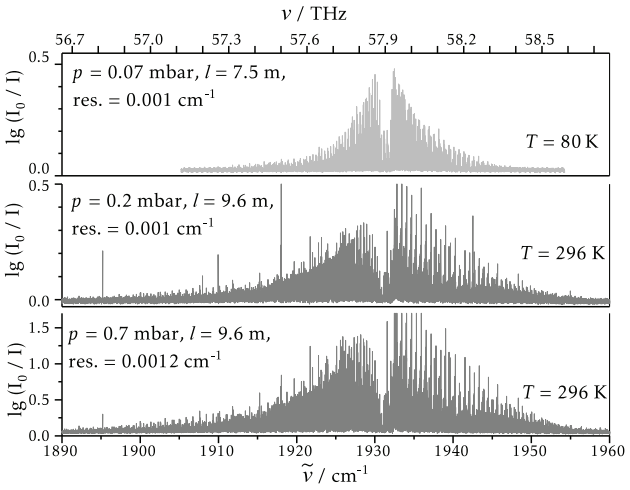


**Fig. 12.** Overview of the $\nu_1 + \nu_3$ band of $NF_3$ measured at room temperature, $T$ = 296 K, (middle and bottom) and at $T$ = 80 K (top trace). The structure of the spectrum is considerably simplified in the low temperature measurements, whereas transitions with high values of $J$ and $K$ are obtained from the spectrum at room temperature. Absorbance is shown as decadic logarithm, $\lg(I_0/I)$. (Top: spectrum I, middle: spectrum VIII, bottom: spectrum XVIII.)

temperature and at $T$ = 120 K is shown in Fig. 13. Other bands of $NF_3$, such as $\nu_1 + 2\nu_4$ ($A_1/E$) and $\nu_2 + \nu_3 + \nu_4$ are observed in this region, but we did not take them into account in our analysis. 924 transitions in the $2\nu_1$ band were assigned up to $J_{max.}$ = 36, $K_{max.}$ = 22 and fitted to a Hamiltonian for an isolated state model giving a set of spectroscopic parameters presented in Table 14.

### 6.2. The $\nu_1 + \nu_2 + \nu_4$ combination band

An overview of the combination band $\nu_1 + \nu_2 + \nu_4$ is shown in Fig. 14. Despite of the relatively weak absorbance in this region, all three branches of the band are clearly visible in both spectra as taken at room temperature and at $T$ = 120 K. The $\nu_1 + \nu_2 + \nu_4$ level is well separated from other bands in the region and is considered here in an approximate isolated state model.

About 820 transitions were assigned in this band with the maximum values for the rotational quantum numbers $J_{max.}$ = 26 and $K_{max.}$ = 25. The parameters of the effective Hamiltonian obtained from the fit are shown in Table 15.

### 6.3. The $\nu_2 + 2\nu_3$ band

The combination band $\nu_2 + 2\nu_3$ has two components of $A_1$ and $E$ symmetry. It has a structure that is similar to the $2\nu_3$ band, which was discussed earlier, see Fig. 15. The absorbance in this range is relatively low and the $(S/N)$ ratio in the low temperature spectrum is low for high $(J,K)$-levels. Moreover, the $E$-component of the $\nu_2 + 2\nu_3$ is predominant in the region and we could not detect the weak lines belonging to the totally symmetric sub-level, $\nu_2 + 2\nu_3$ ($A_1$). About 450 rovibrational transitions were assigned to the $\nu_2 + 2\nu_3$ ($E$) up to $J_{max.} = K_{max.}$ = 36 leading to a set of spectroscopic parameters presented in Tables 16 and 17. The $\nu_2 + 2\nu_3$ ($A_1$) level was considered here as a "dark" state and only the one parameter of the band centre was fitted first. At a later stage of the fit we have also adjusted the rotational constant $B$, which slightly improved the fit. Thus, the final *rms*-deviation was $d_{rms}$ = 0.0005 $cm^{-1}$. Further analysis may be desirable here and is planned.

### 6.4. The $\nu_1 + \nu_2 + \nu_3$ band

The combination band $\nu_1 + \nu_2 + \nu_3$ measured at room temperature and at $T$ = 120 K is shown in Fig. 16. As a result of the high

**Table 13**
Spectroscopic parameters of the $\nu_1 + \nu_3$ vibrational state of $NF_3$ (in $cm^{-1}$).[a]

| Parameter 1 | [34] 2 | This work 3 |
|---|---|---|
| $E^e$ | 1931.577516(19) | 1931.578311(69) |
| $\tilde{\nu}_0$[b] | | 1931.578311(69) |
| $B$ | 0.354822668(77) | 0.35481987(50) |
| $C$ | 0.19368292(12) | 0.19368506(42) |
| $D_J/10^{-6}$ | 0.495089(88) | 0.49525(78) |
| $D_{JK}/10^{-6}$ | −0.77961(22) | −0.78369(163) |
| $D_K/10^{-6}$ | 0.34708(24) | 0.35010(147) |
| $H_J/10^{-11}$ | 0.04687(291) | 0.06135 |
| $H_{JK}/10^{-11}$ | −0.1989(113) | −0.33509 |
| $H_{KJ}/10^{-11}$ | −0.1454(192) | 0.4858 |
| $H_K/10^{-11}$ | 0.8369(150) | −0.10335 |
| $\eta^{\nu E}$,[c] | | 0.3141406(58) |
| $C\zeta$ | 0.15705315(78) | |
| $\eta_J/10^{-5}$ | 0.62304(91) | −0.3253(24) |
| $\eta_K/10^{-5}$ | −0.61512(91) | 0.2885(30) |
| $\eta_{JJ}/10^{-9}$ | −0.3981(18) | |
| $\eta_{JK}/10^{-9}$ | 0.7449(48) | |
| $\eta_{KK}/10^{-9}$ | 0.328(45) | |
| $\tau_{JJJ}/10^{-13}$ | 0.234 | |
| $\tau_{JJK}/10^{-13}$ | −0.768 | |
| $\tau_{JKK}/10^{-13}$ | 0.876 | |
| $\tau_{KKK}/10^{-13}$ | −0.268 | |
| $q/10^{-2}$ | −0.437371(21) | |
| $q_J/10^{-6}$ | 0.11712(28) | |
| $q_{JJ}/10^{-11}$ | −0.6857(92) | |
| $r/10^{-3}$ | 0.24000(37) | |
| $d/10^{-5}$ | 0.0 | |
| $\varepsilon/10^{-6}$ | 0.0 | |
| $f_{42}/10^{-9}$ | 0.815(28) | |
| $\alpha/10^{-2}$ | | −0.1094125(730) |
| $\alpha_J/10^{-6}$ | | 0.3860(152) |
| $\alpha_K/10^{-6}$ | | −0.3961(285) |
| $J_{max.}$ | 55 | 63 |
| $K_{max.}$ | 45 | 45 |
| $N_{tr.}$ | 3282 | 2799 |
| $d_{rms}$ | 0.00034 | 0.00037 |

[a] Values in parentheses are $1\sigma$ standard uncertainties. Parameters presented in column 3 without uncertainties were fixed to the values of the corresponding parameters of the vibrational ground state from Table 4.
[b] $\tilde{\nu}_0$ is the term value of the pure vibrational level ($J$ = 0).
[c] The parameter $\eta^{\nu E}$ can be related to the conventional $C\zeta$ by $\eta^{1E} = 2C\zeta$ for the combination level with one quantum in the degenerate state, [63].

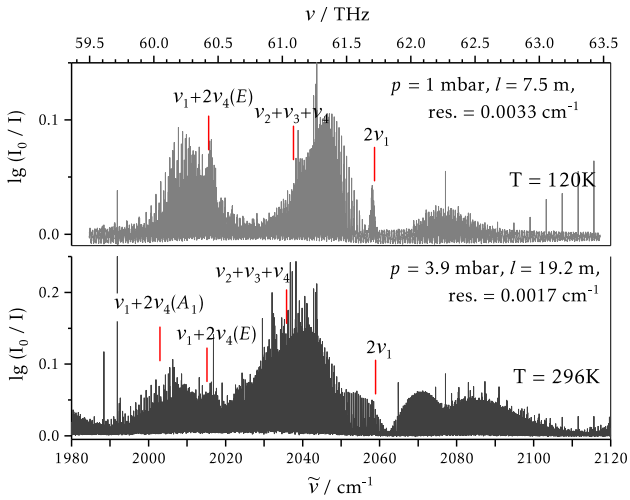


**Fig. 13.** Survey spectrum of the $2\nu_1$ band of $NF_3$ measured at room temperature, $T$ = 296 K, (bottom) and at $T$ = 120 K (top trace). Other combination bands located in the region are marked as well. Absorbance is shown as decadic logarithm, $\lg(I_0/I)$. (Top: spectrum IV, bottom: spectrum XII.)

**Table 14**
Spectroscopic parameters of the $2\nu_1$ level ($A_1$) of $NF_3$ (in $cm^{-1}$).[a]

| Parameter | |
|---|---|
| 1 | 2 |
| $E^a$ | 2058.303839(879) |
| $\tilde{\nu}_0$[b] | 2058.303839(879) |
| $B$ | 0.35616350(205) |
| $C$ | 0.19379787(268) |
| $D_J/10^{-6}$ | 0.51039(963) |
| $D_{JK}/10^{-6}$ | −0.4461(172) |
| $D_K/10^{-6}$ | 0.34343 |
| $H_J/10^{-11}$ | 0.061352 |
| $H_{JK}/10^{-11}$ | −0.3351 |
| $H_{KJ}/10^{-11}$ | 0.4858 |
| $H_K/10^{-11}$ | −0.10335 |
| $J_{max.}$ | 36 |
| $K_{max.}$ | 22 |
| $N_{tr.}$ | 924 |
| $d_{rms}$ | 0.0003 |

[a] Values in parentheses are $1\sigma$ standard uncertainties. Parameters presented without uncertainties were fixed to the values of the corresponding parameters of the vibrational ground state from Section 4.
[b] $\tilde{\nu}_0$ is the term value of the pure vibrational level ($J = 0$).

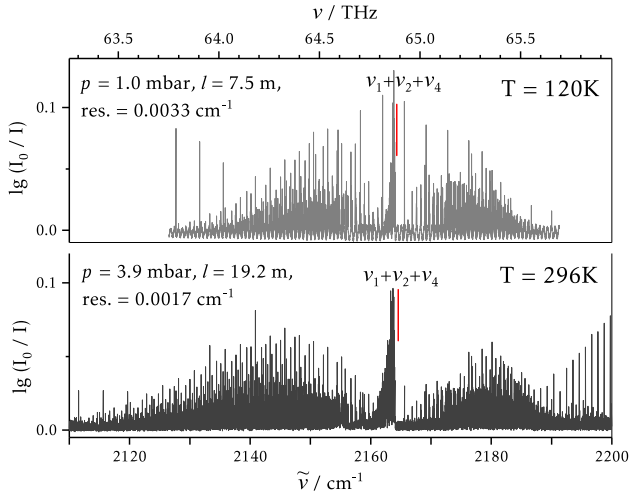


**Fig. 14.** Overview of the spectrum in the region of combination band $\nu_1 + \nu_2 + \nu_4$ of $NF_3$. Absorbance is shown as decadic logarithm, $\lg(I_0/I)$. (Top: spectrum IV, bottom: spectrum XII.)

resolution analysis more than 900 transitions were assigned to the band with $J_{max.} = 28$ and $K_{max.} = 22$. The parameters of the effective hamiltonian obtained from the fitting procedure are presented in Table 18, they reproduce the experimental information about the transitions in the band with an accuracy close to the experimental uncertainties, with a $d_{rms} = 0.00037\ cm^{-1}$. We should point out that the vibrational assignment as $2\nu_1 + \nu_4$ would, in principle, be possible as well, leading, however, to a less good overall description of the vibrational level energies.

### 6.5. The $3\nu_3$ combination band

A survey of the $3\nu_3$ spectrum is shown in Fig. 17 and it looks similar to the combination band $\nu_1 + \nu_3$ discussed above, although, in principle the level $3\nu_3$ is more complex.

A series of lines with $(J, K = J)$ was assigned for the $\Delta K = -1$ sub-band up to $J_{max.} = K_{max.} = 39$, and for $\Delta K = +1$ sub-band the transitions with $J_{max.} = 28$ and $K_{max.} = 25$ were identified. The fitting procedure provided a set of parameters presented in Table 19. For this band also other vibrational assignments are conceivable.

**Table 15**
Spectroscopic parameters of the $\nu_1 + \nu_2 + \nu_4$ vibrational band of $NF_3$ (in $cm^{-1}$)[a].

| Parameter | $\nu_1 + \nu_2 + \nu_4$ |
|---|---|
| 1 | 2 |
| $E^e$ | 2163.874844(13) |
| $\tilde{\nu}_0$[b] | 2163.874844(13) |
| $B$ | 0.356005012(99) |
| $C$ | 0.19291297(15) |
| $D_J/10^{-6}$ | 0.6225(21) |
| $D_{JK}/10^{-6}$ | −0.6052(77) |
| $D_K/10^{-6}$ | 0.6246(86) |
| $H_J/10^{-11}$ | 0.061352 |
| $H_{JK}/10^{-11}$ | −0.33510 |
| $H_{KJ}/10^{-11}$ | 0.4858 |
| $H_K/10^{-11}$ | −0.10335 |
| $\eta^{\nu E c)}$ | −0.3295397(36) |
| $\eta_J/10^{-4}$ | 0.1071(46) |
| $\eta_K/10^{-5}$ | 0.231(52) |
| $\eta_{JJ}/10^{-8}$ | −0.701(61) |
| $\eta_{JK}/10^{-7}$ | 0.257(18) |
| $\eta_{KK}/10^{-8}$ | −0.545(158) |
| $\alpha/10^{-3}$ | 0.40421(35) |
| $\alpha_J/10^{-7}$ | −0.2935(81) |
| $\alpha_K/10^{-7}$ | −0.204(11) |
| $J_{max.}$ | 26 |
| $K_{max.}$ | 25 |
| $N_{tr.}$ | 828 |
| $d_{rms}$ | 0.0006 |

[a] Values in parentheses are $1\sigma$ standard uncertainties. Parameters presented without uncertainties were fixed to the values of the corresponding parameters of the vibrational ground state from Table 4.
[b] $\tilde{\nu}_0$ is the term value of the pure vibrational level ($J = 0$).
[c] The parameter $\eta^{\nu E}$ can be related to the conventional $C\zeta$ by $\eta^{1E} = 2C\zeta$ for the fundamental and for the combination band with one quantum in the degenerate vibration, [63].

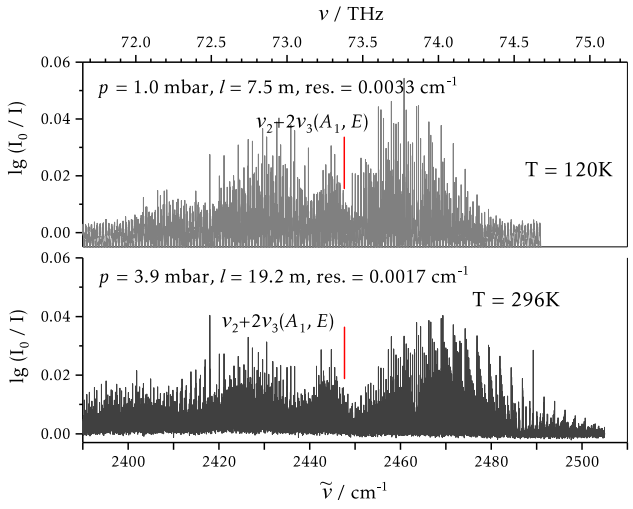


**Fig. 15.** Overview of the $\nu_2 + 2\nu_3$ band of $NF_3$ measured at room temperature, $T = 296$ K, (bottom) and at $T = 120$ K (top trace). The fringes in the low temperature spectrum arise due to reflection effects on the optical elements, but due to their relatively large period this does not affect structure of the spectrum importantly. Absorbance is shown as decadic logarithm, $\lg(I_0/I)$. (Top: spectrum IV, bottom: spectrum XII.)

### 6.6. The $\nu_1 + 2\nu_3$ band

The $\nu_1 + 2\nu_3$ ($A_1/E$) band is located around 2820 $cm^{-1}$. Similar to the case of the $\nu_2 + 2\nu_3$ band, the $E$-component dominates in the spectrum and we could not obtain the lines belonging to the

**Table 16**
Spectroscopic parameters of the $\nu_2 + 2\nu_3$ levels of $NF_3$[a].

| Parameter 1 | $\nu_2 + 2\nu_3$ ($A_1$) 2 | $\nu_2 + 2\nu_3$ ($E$) 3 |
|---|---|---|
| $E^{a,e}$ | 2447.5511(22) | 2445.31168(82) |
| $\tilde{\nu}_0$[b] | 2447.5511(22) | 2445.31168(82) |
| $B$ | 0.354586(77) | 0.35007442(65) |
| $C$ | 0.19499250 | 0.1933619(53) |
| $D_J/10^{-6}$ | 0.48733446 | 0.13688(88) |
| $D_{JK}/10^{-6}$ | −0.7596562 | −1.7006(207) |
| $D_K/10^{-6}$ | 0.34343 | 1.076(901) |
| $H_J/10^{-11}$ | 0.061352 | 0.061352 |
| $H_{JK}/10^{-11}$ | −0.33510 | −0.33510 |
| $H_{KJ}/10^{-11}$ | 0.4858 | 0.4858 |
| $H_K/10^{-11}$ | −0.10335 | −0.10335 |
| $\eta^{\nu E}$[c] | | −0.5989288(804) |
| $\eta_J/10^{-4}$ | | 0.419(15) |
| $\eta_K/10^{-3}$ | | 0.1105(35) |
| $J_{max.}$ | | 36 |
| $K_{max.}$ | | 36 |
| $N_{tr.}$ | | 457 |
| $d_{rms}$ | | 0.0005 |

[a] Values in parentheses are $1\sigma$ standard uncertainties. Parameters presented without uncertainties were fixed to the values of the corresponding parameters of the ground state from Table 4.
[b] $\tilde{\nu}_0$ is the term value of the pure vibrational level ($J = 0$).
[c] The parameter $\eta^{\nu E}$ can be related to the conventional $C\zeta$ by $\eta^{2E} = -4C\zeta$ for the combination band with two quanta in the degenerate state, [63].

**Table 17**
Interaction parameters between $\nu_2 + 2\nu_3$ ($A_1$) and $\nu_2 + 2\nu_3$ ($E$) vibrational states of $NF_3$ (in $cm^{-1}$)[a].

| Parameter 1 | 2 |
|---|---|
| $\tilde{\alpha}/10^{-2}$ | 0.8456(55) |
| $\tilde{\alpha}_J/10^{-5}$ | 0.477(54) |
| $\tilde{\alpha}_K/10^{-4}$ | −0.838(16) |

[a] Values in parentheses are $1\sigma$ standard uncertainties.

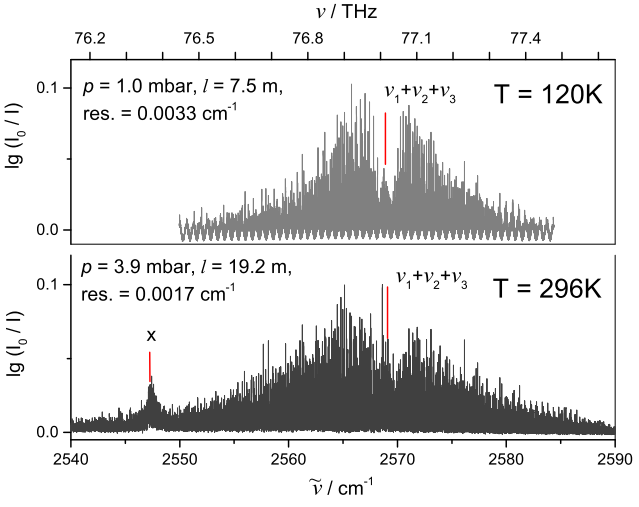


**Fig. 16.** Overview of the spectrum in the region of combination band $\nu_1 + \nu_2 + \nu_3$ of $NF_3$. The $Q$-branch of another (unidentified) band is seen in the room temperature spectrum. Spectrum IV in Table 2 is shown on top of the Figure and spectrum XII is shown on the bottom. Absorbance is shown as decadic logarithm, $\lg(I_0/I)$.

$\nu_1 + 2\nu_3$ ($A_1$) band. From the assignment of the transitions in the low temperature spectrum (Fig. 18) about 900 were obtained with maximum values for the rotational quantum numbers $J_{max.} = 40$ and $K_{max.} = 39$.

**Table 18**
Spectroscopic parameters of the $\nu_1 + \nu_2 + \nu_3$ vibrational band of $NF_3$ (in $cm^{-1}$)[a].

| Parameter 1 | $\nu_1 + \nu_2 + \nu_3$ 2 |
|---|---|
| $E^e$ | 2569.25487(68) |
| $\tilde{\nu}_0$[b] | 2569.25487(68) |
| $B$ | 0.3536727(48) |
| $C$ | 0.1937607(63) |
| $D_J/10^{-6}$ | 0.3965(75) |
| $D_{JK}/10^{-6}$ | −1.277(17) |
| $D_K/10^{-6}$ | 0.109(13) |
| $H_J/10^{-11}$ | 0.061352 |
| $H_{JK}/10^{-11}$ | −0.33510 |
| $H_{KJ}/10^{-11}$ | 0.4858 |
| $H_K/10^{-11}$ | −0.10335 |
| $\eta^{\nu E}$[c] | 0.2934367(48) |
| $\eta_J/10^{-4}$ | −0.1699(14) |
| $\eta_K/10^{-4}$ | −0.1240(16) |
| $\alpha/10^{-7}$ | 0.9751(15) |
| $J_{max.}$ | 28 |
| $K_{max.}$ | 22 |
| $N_{tr.}$ | 905 |
| $d_{rms}$ | 0.00037 |

[a] Values in parentheses are $1\sigma$ standard uncertainties. Parameters presented without uncertainties were fixed to the values of the corresponding parameters of the vibrational ground state from Table 4.
[b] $\tilde{\nu}_0$ is the term value of the pure vibrational level ($J = 0$).
[c] The parameter $\eta^{\nu E}$ can be related to the conventional $C\zeta$ by $\eta^{1E} = 2C\zeta$ for the combination with one quantum in the degenerate vibration, [63].

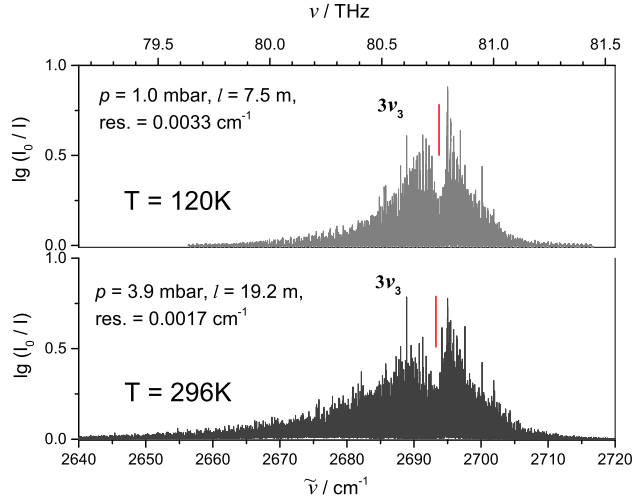


**Fig. 17.** Survey spectrum of the $3\nu_3$ band of $NF_3$ measured at room temperature, $T$ = 296 K, (bottom) and at $T$ = 120 K (top trace). Absorbance is shown as decadic logarithm, $\lg(I_0/I)$. (Top: spectrum IV, bottom: spectrum XII).

Following the fitting procedure that was exploited for the case of $\nu_2 + 2\nu_3$, we have treated the $\nu_1 + 2\nu_3$ ($A_1$) level as a "dark" state. Only the parameter of the band centre was adjusted in the fit, while the other parameters were fixed to the values of the corresponding parameters of the vibrational ground state. Only at the last stage of the fitting the rotational constant $B$ was adjusted as well resulting in an improved $d_{rms} = 0.00044\ cm^{-1}$. One should note that the analysis can be further improved by including the transitions with higher $J$ and $K$ values and possibly the transitions belonging to the totally symmetric component, if assigned. The present results are summarised in Table 20 and Table 21.

## 7. Conclusions

We have studied the high resolution spectra of thirteen rovibrational bands of $NF_3$ measured at room temperature and at low tem-

**Table 19**
Spectroscopic parameters of the $3\nu_3$ level ($E$) of $NF_3$ (in $cm^{-1}$)[a].

| Parameter 1 | 2 |
|---|---|
| $E^e$ | 2694.122859(545) |
| $\tilde{\nu}_0$[b] | 2694.122859(545) |
| $B$ | 0.34912257(211) |
| $C$ | 0.19274626(139) |
| $D_J/10^{-6}$ | 0.22543(115) |
| $D_{JK}/10^{-6}$ | −0.43760(152) |
| $D_K/10^{-6}$ | 0.13127(797) |
| $H_J/10^{-11}$ | 0.06135 |
| $H_{JK}/10^{-11}$ | −0.33509 |
| $H_{KJ}/10^{-11}$ | 0.4858 |
| $H_K/10^{-11}$ | −0.10335 |
| $\eta^{\nu E c)}$ | 0.3018318(642) |
| $\eta_J/10^{-5}$ | 0.4290(43) |
| $\alpha/10^{-2}$ | 0.187544(58) |
| $\alpha_J/10^{-5}$ | 0.315(200) |
| $J_{max.}$ | 39 |
| $K_{max.}$ | 39 |
| $N_{tr.}$ | 403 |
| $d_{rms}$ | 0.00032 |

[a] Values in parentheses are $1\sigma$ standard uncertainties. Parameters presented without uncertainties were fixed to the values of the corresponding parameters of the vibrational ground state.
[b] $\tilde{\nu}_0$ is the term value of the pure vibrational level ($J = 0$).
[c] The parameter $\eta^{\nu E}$ can be related to the conventional $C\zeta$ [63].

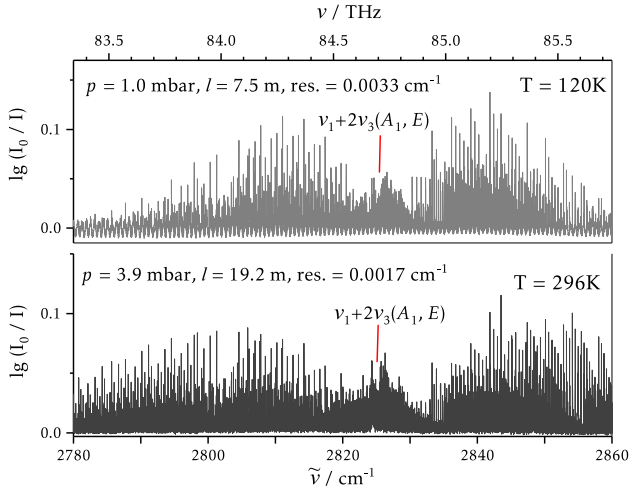


**Fig. 18.** Overview of the $\nu_1 + 2\nu_3$ ($A_1/E$) band of $NF_3$ measured at room temperature, $T = 296$ K, (bottom) and at $T = 120$ K (top trace). The doubly-degenerate component, $\nu_1 + 2\nu_3$ ($E$), is predominant in the spectrum. Absorbance is shown as decadic logarithm, $\lg(I_0/I)$. (Top: spectrum IV, bottom: spectrum XII.)

**Table 20**
Spectroscopic parameters of the $\nu_1 + 2\nu_3$ vibrational levels ($A_1/E$) of $NF_3$ (in $cm^{-1}$)[a].

| Parameter 1 | $\nu_1 + 2\nu_3$ ($A_1$) 2 | $\nu_1 + 2\nu_3$ ($E$) 3 |
|---|---|---|
| $E^{a,e}$ | 2820.10230(502) | 2826.18192(44) |
| $\tilde{\nu}_0$[b] | 2820.10230(502) | 2826.18192(44) |
| $B$ | 0.352485(21) | 0.3519729(70) |
| $C$ | 0.1931280(91) | 0.1929189(20) |
| $D_J/10^{-6}$ | 0.48733446 | 0.48733446 |
| $D_{JK}/10^{-6}$ | −0.7596562 | −0.7596562 |
| $D_K/10^{-6}$ | 0.34343 | 0.34343 |
| $H_J/10^{-11}$ | 0.061352 | 0.061352 |
| $H_{JK}/10^{-11}$ | −0.33510 | −0.33510 |
| $H_{KJ}/10^{-11}$ | 0.4858 | 0.4858 |
| $H_K/10^{-11}$ | −0.10335 | −0.10335 |
| $\eta^{\nu E c)}$ | | −0.6180799(456) |
| $\eta_J/10^{-4}$ | | 0.677(82) |
| $\eta_K/10^{-4}$ | | 0.626(86) |
| $\eta_{JJ}/10^{-7}$ | | −0.0361(70) |
| $\eta_{JK}/10^{-7}$ | | 0.164(22) |
| $\eta_{KK}/10^{-7}$ | | −0.127(16) |
| $J_{max.}$ | | 40 |
| $K_{max.}$ | | 39 |
| $N_{l.}$ | | 909 |
| $d_{rms}$ | 0.0039 | |

[a] Values in parentheses are $1\sigma$ standard uncertainties. Parameters presented without uncertainties were fixed to the values of the corresponding parameters of the vibrational ground state from Table 4.
[b] $\tilde{\nu}_0$ is the term value of the pure vibrational level ($J = 0$).
[c] The parameter $\eta^{\nu E}$ can be related to the conventional $C\zeta$ by $\eta^{2E} = -4C\zeta$ for the combination with two quanta in the degenerate vibration, [63].

**Table 21**
Interaction parameters between $\nu_1 + 2\nu_3$ ($A_1$) and $\nu_1 + 2\nu_3$ ($E$) vibrational states of the $NF_3$ (in $cm^{-1}$)[a].

| Parameter 1 | 2 |
|---|---|
| $\tilde{\alpha}/10^{-2}$ | 0.691(171) |
| $\tilde{\alpha}_J/10^{-5}$ | 0.622(137) |
| $\tilde{\alpha}_K/10^{-4}$ | −0.173(13) |
| $\tilde{\alpha}_{JJ}/10^{-8}$ | −0.169(45) |
| $\tilde{\alpha}_{KK}/10^{-8}$ | 0.724(71) |
| $\tilde{\beta}/10^{-3}$ | 0.337(24) |
| $\tilde{\beta}_J/10^{-6}$ | −0.110(21) |
| $\tilde{\beta}_K/10^{-6}$ | 0.378(36) |
| $\tilde{\gamma}/10^{-2}$ | 0.20420(48) |
| $\tilde{\gamma}_J/10^{-7}$ | −0.292(106) |

[a] Values in parentheses are $1\sigma$ standard uncertainties.

peratures, between $T = 80$ K and $T = 120$ K, thus covering the temperature ranges of relevance for the Earth's atmosphere and beyond. This rather comprehensive analysis of the spectral range from 1000 to 3000 $cm^{-1}$ allowed us to extend the spectroscopic information available before substantially for the bands in the region 800–2000 $cm^{-1}$ ($2\nu_4, \nu_1, \nu_2 + \nu_4, \nu_1 + \nu_4, \nu_2 + \nu_3, 2\nu_3$ and $\nu_1 + \nu_3$). We furthermore obtained new results for the rovibrational bands located in the wavenumber range from 2000 to 3000 $cm^{-1}$. The rovibrational transitions in the high resolution spectra were newly assigned to the $2\nu_1, \nu_1 + \nu_2 + \nu_4, \nu_2 + 2\nu_3$, $\nu_1 + \nu_2 + \nu_3, 3\nu_3$ and $\nu_1 + 2\nu_3$ bands, where such assignments have only approximate meaning as zero order contributions and a few of the vibrational assignments remain tentative.

Table 22 provides a survey of the energy levels redetermined and newly determined here. These results increase the spectroscopic data base useful for the atmospheric trace gas spectroscopy of $NF_3$ very importantly and can be used as a starting point for further, more detailed studies in selected wavenumber ranges and for the extension of the analyses to even higher energies.

The extensive results obtained here also increase our understanding of the rovibrational dynamics of $NF_3$ towards higher vibrational excitations. It turns out that the vibrational levels under consideration can formally be analyzed as almost isolated, with some modest interactions but without the very strong couplings, which dominate the spectra of $NH_3$ [65,66] and $CHF_3$ [53–55]. Nevertheless, this observation does not exclude that in actual

**Table 22**
Analyzed vibrational energy levels of $NF_3$ (in $cm^{-1}$)[b].

| Parameter 1 | $v_0^{exp}$ 2 | $v_0^{calc}$ 3 |
|---|---|---|
| $\nu_4$ ($E$) | 493.42[a] | 493.19 |
| $\nu_2$ ($A_1$) | 647.13[a] | 646.08 |
| $\nu_3$ ($E$) | 907.54[a] | 907.439 |
| $2\nu_4$ ($A_1$) | 983.70139 | 983.658 |
| $2\nu_4$ ($E$) | 986.62267 | 986.658 |
| $\nu_1$ ($A_1$) | 1032.0014193 | 1031.867 |
| $\nu_2 + \nu_4$ ($E$) | 1138.2766 | 1138.508 |
| $\nu_1 + \nu_4$ ($E$) | 1523.3048611 | 1523.467 |
| $\nu_2 + \nu_3$ ($E$) | 1548.2717812 | 1550.249 |
| $2\nu_3$ ($A_1$) | 1803.130641 | 1804.382 |
| $2\nu_3$ ($E$) | 1810.424372 | 1808.378 |
| $\nu_1 + \nu_3$ ($E$) | 1931.578311 | 1931.653 |
| $2\nu_1$ ($A_1$) | 2058.303839 | 2058.297 |
| $\nu_1 + \nu_2 + \nu_4$ ($E$) | 2163.874844 | 2163.728 |
| $\nu_2 + 2\nu_3$ ($A_1$) | 2447.55110 | 2443.923 |
| $\nu_2 + 2\nu_3$ ($E$) | 2445.31168 | 2447.919 |
| $\nu_1 + \nu_2 + \nu_3$ ($E$) | 2569.25487 | 2569.407 |
| $3\nu_3$ ($E$) | 2694.122859 | 2694.825 |
| $\nu_1 + 2\nu_3$ ($A_1$) | 2820.10230 | 2820.945 |
| $\nu_1 + 2\nu_3$ ($E$) | 2826.18192 | 2824.941 |

[a] Values taken from reference [20].
[b] The calculation is carried out with the following parameters from a best fit with the simple term formula: $\omega_1 = 1049.073, \omega_2 = 654.401, \omega_3 = 929.768, \omega_4 = 500.569, x_{11} = -2.718, x_{22} = -0.88, x_{33} = -4.249, x_{44} = -0.611, x_{12} = -5.057, x_{13} = -7.652, x_{14} = -1.59, x_{23} = -3.27, x_{24} = -0.762, x_{34} = -5.12, g_{33} = 0.999, g_{34} = -0.1, g_{44} = 0.75$ (all values in $cm^{-1}$) (term formula including zero point energies being used, see Ref. [67]).

fact there are sizeable anharmonic and rovibrational interactions, as can be estimated from ab initio results [19]. For instance, while most of the rotational constants for combination and overtone levels show the behaviour expected from theory, for $2\nu_1$ there are substantial differences with respect to the B constant, which may be indicative of interactions with neighboring levels. A similar situation also arises for $\nu_2 + 2\nu_3$, which is also fitted less well by the simple term formula. The parameters of the simple anharmonic term formulae and the rotational parameters have thus only an effective meaning and a more detailed analysis of the spectrum of interacting levels including input from theory is planned. Also, as expected from theory, there is no evidence for inversion tunneling in $NF_3$ even at the highest energies investigated here.

## Acknowledgment

Our work is supported by the Swiss National Science Foundation and the ETH Zurich (in particular the Laboratory of Physical Chemistry) as well as COST MOLIM. We enjoyed discussions with Frédéric Merkt, Carine Manca Tanner, Ziqiu Chen, Lubos Horny, and Csaba Fábri. Part of the research was funded by the Russian Science Foundation project No. 18-12-00058.

## Appendix A. Supplementary material

The supplementary data associated with this article contain 15 tables of lines and can be found in the online version at http://dx.doi.org/10.1016/j.jms.2018.04.004.

## References

[1] J. Sheridan, W. Gordy, Phys. Rev. 79 (1950) 513–515, https://doi.org/10.1103/PhysRev.79.513.
[2] C.M. Johnson, R. Trambarulo, W. Gordy, Phys. Rev. 84 (1951) 1178–1180, https://doi.org/10.1103/PhysRev.84.1178.
[3] M. Cowan, W. Gordy, Bull. Am. Phys. Soc. 5 (1960) 241.
[4] P. Kisliuk, J. Chem. Phys. 22 (1954) 86–92, https://doi.org/10.1063/1.1739863.
[5] A.M. Mirri, G. Cazzoli, J. Chem. Phys. 47 (1967) 1197–1198, https://doi.org/10.1063/1.1712047.
[6] A.M. Mirri, J. Chem. Phys. 47 (1967) 2823–2828, https://doi.org/10.1063/1.1712304.
[7] M. Otake, C. Matsumura, Y. Morino, J. Mol. Spectrosc. 28 (1968) 316–324, https://doi.org/10.1016/0022-2852(68)90078-7. <http://www.sciencedirect.com/science/article/pii/0022285268900787>.
[8] M. Otake, E. Hirota, Y. Morino, J. Mol. Spectrosc. 28 (1968) 325–340, https://doi.org/10.1016/0022-2852(68)90079-9. <http://www.sciencedirect.com/science/article/pii/0022285268900799>.
[9] R.G. Stone, J.M. Pochan, W.H. Flygare, Inorgan. Chem. 8 (1969) 2647–2655, https://doi.org/10.1021/ic50082a021.
[10] G. Cazzoli, L. Cludi, C.D. Esposti, L. Dore, J. Mol. Spectrosc. 152 (1992) 185–191, https://doi.org/10.1016/0022-2852(92)90129-C. <http://www.sciencedirect.com/science/article/pii/002228529290129C>.
[11] A. Schmiedekamp, S. Skaarup, P. Pulay, J.E. Boggs, J. Chem. Phys. 66 (1977) 5769–5776, https://doi.org/10.1063/1.433852. <http://scitation.aip.org/content/aip/journal/jcp/66/12/10.1063/1.433852>.
[12] D.S. Marynick, J. Chem. Phys. 73 (1980) 3939–3943, https://doi.org/10.1063/1.440579. <http://scitation.aip.org/content/aip/journal/jcp/73/8/10.1063/1.440579>.
[13] D.S. Marynick, D.C. Rosen, J.F. Liebman, J. Mol. Struct. 94 (1983) 47–50, https://doi.org/10.1016/0022-2860(83)90260-0. <http://www.sciencedirect.com/science/article/pii/0022286083902600>.
[14] P. Schwerdtfeger, P.D.W. Boyd, T. Fischer, P. Hunt, M. Liddell, J. Am. Chem. Soc. 116 (1994) 9620–9633, https://doi.org/10.1021/ja00100a029.
[15] J.I. Robson, L.K. Gohar, M.D. Hurley, K.P. Shine, T.J. Wallington, Geophys. Res. Lett. 33 (2006) n/a–n/a.
[16] M.J. Prather, J. Hsu, Geophys. Res. Lett. 35 (2008) 1–3, https://doi.org/10.1029/2008GL034542.
[17] R.F. Weiss, J. Mühle, P.K. Salameh, C.M. Harth, Geophys. Res. Lett. 35 (2008) n/a–n/a, https://doi.org/10.1029/2008GL035913.
[18] T. Arnold, C.M. Harth, J. Mühle, A.J. Manning, P.K. Salameh, J. Kim, D.J. Ivy, L.P. Steele, V.V. Petrenko, J.P. Severinghaus, D. Baggenstos, R.F. Weiss, Proc. Nat. Acad. Sci. 110 (2013) 2029–2034, https://doi.org/10.1073/pnas.1212346110. arXiv:http://www.pnas.org/content/110/6/2029.full.pdf <http://www.pnas.org/content/110/6/2029.abstract>.
[19] J. Breidung, L. Constantin, J. Demaison, L. Margulès, W. Thiel, Mol. Phys. 101 (2003) 1113–1122, https://doi.org/10.1080/0026897031000068532.
[20] H. Najib, J. Mol. Spectrosc. 312 (2015) 1–5.
[21] W.G. Golden, C.C. Blackburn, J. Overend, Spectrochim. Acta Part A: Mol. Spectrosc. 33 (1977) 901–906, https://doi.org/10.1016/0584-8539(77)80089-5. A.J. II <http://www.sciencedirect.com/science/article/pii/0584853977800895>.
[22] R. Popplewell, F. Masri, H. Thompson, Spectrochim. Acta Part A: Mol. Spectrosc. 23 (1967) 2797–2807, https://doi.org/10.1016/0584-8539(67)80172-7. <http://www.sciencedirect.com/science/article/pii/0584853967801727>.
[23] G.W. Chantry, H.A. Gebbie, Proc. Roy. Soc. Lond. A: Math. Phys. Eng. Sci. 304 (1968) 45–51.
[24] S. Reichman, S. Ginn, J. Mol. Spectrosc. 40 (1971) 27–32, https://doi.org/10.1016/0022-2852(71)90004-X. <http://www.sciencedirect.com/science/article/pii/002228527190004X>.
[25] S. Reichman, J. Schatz, J. Mol. Spectrosc. 48 (1973) 277–282, https://doi.org/10.1016/0022-2852(73)90192-6. <http://www.sciencedirect.com/science/article/pii/0022285273901926>.
[26] W. Höhe, W. Kreiner, J. Mol. Spectrosc. 150 (1991) 28–32, https://doi.org/10.1016/0022-2852(91)90190-L. <http://www.sciencedirect.com/science/article/pii/002228529190190L>.
[27] W. Höhe, U. Häring, W.A. Kreiner, H. Essig, A. Ruoff, Can. J. Phys. 72 (1994) 1051–1059, https://doi.org/10.1139/p94-137.
[28] S.E. Novick, W. Chen, M.R. Munrow, K.J. Grant, J. Mol. Spectrosc. 179 (1996) 219–222, https://doi.org/10.1006/jmsp.1996.0199. <http://www.sciencedirect.com/science/article/pii/S002228529690199X>.
[29] N. Boulaftali, N. Sari-Zizi, U. Wötzel, J. Demaison, L. Margulès, H. Harder, H. Mäder, E. MKadmi, H. Bürger, J. Mol. Spectrosc. 212 (2002) 41–52, https://doi.org/10.1006/jmsp.2001.8505. <http://www.sciencedirect.com/science/article/pii/S0022285201985054>.
[30] H. Najib, N.B. Sari-Zizi, J. Demaison, B. Bakri, J.-M. Colmont, E. MKadmi, J. Mol. Spectrosc. 220 (2003) 214–222, https://doi.org/10.1016/S0022-2852(03)00127-9. <http://www.sciencedirect.com/science/article/pii/S0022285203001279>.
[31] K. Akkad, N.B. Sari-Zizi, B. Bakri, J. Demaison, H. Bürger, E. MKadmi, J. Mol. Spectrosc. 218 (2003) 36–47, https://doi.org/10.1016/S0022-2852(02)00028-0. <http://www.sciencedirect.com/science/article/pii/S0022285202000280>.
[32] N.B. Sari-Zizi, H. Najib, J. Demaison, B. Bakri, J. Colmont, H. Bürger, J. Mol. Spectrosc. 228 (2004) 511–527, https://doi.org/10.1016/j.jms.2004.07.010 (special Issue Dedicated to Dr. Jon T. Hougen on the Occasion of His 68th Birthday) <http://www.sciencedirect.com/science/article/pii/S002228520400236X>.
[33] G. Cazzoli, C. Puzzarini, J. Mol. Spectrosc. 239 (2006) 59–63, https://doi.org/10.1016/j.jms.2006.05.018. <http://www.sciencedirect.com/science/article/pii/S0022285206001731>.
[34] N.B. Sari-Zizi, H. Najib, J. Mol. Spectrosc. 240 (2006) 210–226, https://doi.org/10.1016/j.jms.2006.09.011. <http://www.sciencedirect.com/science/article/pii/S002228520600258X>.
[35] S. Hmimou, H. Msahal, H. Najib, Mol. Phys. 108 (2010) 787–794, https://doi.org/10.1080/00268971003662904.
[36] H. Najib, S. Hmimou, H. Msahal, E-J. Chem. 9 (2012) 253–259, https://doi.org/10.1155/2012/218684.

[37] H. Najib, Sci. World J. 2013 (2013) 5, https://doi.org/10.1155/2013/813249.
[38] I.W. Levin, S. Abramowitz, J. Chem. Phys. 44 (1966) 2562–2567, https://doi.org/10.1063/1.1727093. <http://scitation.aip.org/content/aip/journal/jcp/44/7/10.1063/1.1727093>.
[39] D.C. Ghosh, J. Jana, S. Bhattacharyya, Int. J. Quant. Chem. 87 (2002) 111–134, https://doi.org/10.1002/qua.10087.
[40] I.W. Levin, J. Chem. Phys. 52 (1970) 2783–2784, https://doi.org/10.1063/1.1673382. <http://scitation.aip.org/content/aip/journal/jcp/52/5/10.1063/1.1673382>.
[41] D. Berckmans, H. Figeys, P. Geerlings, J. Mol. Struct.: THEOCHEM 149 (1987) 243–257, https://doi.org/10.1016/0166-1280(87)87024-0. <http://www.sciencedirect.com/science/article/pii/0166128087870240>.
[42] R. Tarroni, P. Palmieri, M.L. Senent, A. Willetts, Chem. Phys. Lett. 257 (1996) 23–30, https://doi.org/10.1016/0009-2614(96)00526-X. <http://www.sciencedirect.com/science/article/pii/000926149600526X>.
[43] I. Bolotova, O. Ulenikov, S. Albert, S. Bauerecker, P. Lerch, M. Quack, T. Peter, A. Wokaun, in: J. Stohner, C. Yeretzian (Eds.), XXth Symposium on Atomic, Cluster and Surface Physics 2016 (SASP 2016), SASP, Universität Innsbruck, Innsbruck University Press, Davos, Switzerland, 2016, pp. 173–176.
[44] I.B. Bolotova, High Resolution Fourier-Transform Infrared Spectroscopy and Quantum Dynamics of Polyatomic Molecules, Dissertation ETH Nr. 24124, Eidgenössische Technische Hochschule Zürich (ETH Zürich), Zürich, 2017.
[45] I. Bolotova, L. Horný, M. Quack, 2018 (in preparation).
[46] M.J. Frisch, G.W. Trucks, H.B. Schlegel, G.E. Scuseria, M.A. Robb, J.R. Cheeseman, G. Scalmani, V. Barone, B. Mennucci, G.A. Petersson, H. Nakatsuji, M. Caricato, X. Li, H.P. Hratchian, A.F. Izmaylov, J. Bloino, G. Zheng, J.L. Sonnenberg, M. Hada, M. Ehara, K. Toyota, R. Fukuda, J. Hasegawa, M. Ishida, T. Nakajima, Y. Honda, O. Kitao, H. Nakai, T. Vreven, J.A. Montgomery, Jr., J.E. Peralta, F. Ogliaro, M. Bearpark, J.J. Heyd, E. Brothers, K.N. Kudin, V.N. Staroverov, R. Kobayashi, J. Normand, K. Raghavachari, A. Rendell, J.C. Burant, S.S. Iyengar, J. Tomasi, M. Cossi, N. Rega, J.M. Millam, M. Klene, J.E. Knox, J.B. Cross, V. Bakken, C. Adamo, J. Jaramillo, R. Gomperts, R.E. Stratmann, O. Yazyev, A.J. Austin, R. Cammi, C. Pomelli, J.W. Ochterski, R.L. Martin, K. Morokuma, V.G. Zakrzewski, G.A. Voth, P. Salvador, J.J. Dannenberg, S. Dapprich, A.D. Daniels, Ö. Farkas, J.B. Foresman, J.V. Ortiz, J. Cioslowski, D.J. Fox, Gaussian09 Revision E.01, Gaussian Inc. Wallingford CT 2009, 2009.
[47] S. Albert, K.K. Albert, M. Quack, in: M. Quack, F. Merkt (Eds.), Handbook of High-resolution Spectroscopy, vol. 2, John Wiley & Sons, Ltd, 2011, pp. 965–1019, https://doi.org/10.1002/9780470749593.hrs042.
[48] S. Albert, S. Bauerecker, M. Quack, A. Steinlin, Mol. Phys. 105 (2007) 541–558, https://doi.org/10.1080/00268970601164198. arXiv:http://www.tandfonline.com/doi/pdf/10.1080/00268970601164198 <http://www.tandfonline.com/doi/abs/10.1080/00268970601164198>.
[49] S. Albert, K. Keppler, P. Lerch, M. Quack, A. Wokaun, J. Mol. Spectrosc. 315 (2015) 92–101.
[50] S. Albert, K.K. Albert, P. Lerch, M. Quack, Faraday Discuss. 150 (2011) 71–99, https://doi.org/10.1039/C0FD00013B.
[51] S. Bauerecker, M. Taraschewski, C. Weitkamp, H.K. Cammenga, Rev. Sci. Instrum. 72 (2001) 3946–3955, https://doi.org/10.1063/1.1400158. <http://scitation.aip.org/content/aip/journal/rsi/72/10/10.1063/1.1400158>.
[52] H. Longuet-Higgins, Mol. Phys. 6 (1963) 445–460, https://doi.org/10.1080/00268976300100501.
[53] S. Albert, S. Bauerecker, E. Bekhtereva, I. Bolotova, H. Hollenstein, M. Quack, O. Ulenikov, Mol. Phys. 116 (2018) 1091, https://doi.org/10.1080/00268976.2017.1392628.
[54] I. Bolotova, O. Ulenikov, E. Bekhtereva, S. Albert, Z. Chen, H. Hollenstein, D. Zindel, M. Quack, J. Mol. Spectrosc. 337 (2017) 96–104.
[55] S. Albert, E. Bekhtereva, I. Bolotova, Z. Chen, C. Fabri, H. Hollenstein, M. Quack, O. Ulenikov, Phys. Chem. Chem. Phys. 19 (2017) 26527–26534, https://doi.org/10.1039/C7CP04762B.
[56] P. Dietiker, E. Miloglyadov, M. Quack, A. Schneider, G. Seyfang, J. Chem. Phys. 143 (2015) 244305.
[57] M. Quack, Mol. Phys. 34 (1977) 477–504.
[58] M. Quack, Fundamental symmetries and symmetry violations from High Resolution Spectroscopy, in: Handbook of High-resolution Spectroscopy, vol. 1, John Wiley & Sons, Ltd, 2011, pp. 659–722.
[59] O. Ulenikov, A. Malikova, S. Alanko, M. Koivusaari, R. Anttila, J. Mol. Spectrosc. 179 (1996) 175–194. <http://www.sciencedirect.com/science/article/pii/S0022285296901964>.
[60] O. Ulenikov, G. Onopenko, N. Tyabaeva, S. Alanko, M. Koivusaari, R. Anttila, J. Mol. Spectrosc. 186 (1997) 293–313, https://doi.org/10.1006/jmsp.1997.7431. <http://www.sciencedirect.com/science/article/pii/S0022285297974312>.
[61] D. Papoušek, M.R. Aliev, Molecular Vibrational and Rotational Spectra, vol. 5, Elsevier Scientific Publishing Co., Amsterdam, Oxford, New York, 1982.
[62] J.K. Watson, Aspects of Quartic and Sextic Centrifugal Effects on Rotational Energy Levels, vol. 6, Elsevier, Amsterdam, The Netherlands, 1977.
[63] O. Ulenikov, E. Bekhtereva, A. Fomchenko, A. Litvinovskaya, C. Leroy, M. Quack, Mol. Phys. 112 (2014) 2529–2556, https://doi.org/10.1080/00268976.2014.912360.
[64] F. Masri, W. Blass, J. Mol. Spectrosc. 39 (1971) 98–114, https://doi.org/10.1016/0022-2852(71)90281-5. <http://www.sciencedirect.com/science/article/pii/0022285271902815>.
[65] M. Snels, H. Hollenstein, M. Quack, J. Mol. Spectrosc. 237 (2006) 143–148, https://doi.org/10.1016/j.jms.2006.03.006. <http://www.sciencedirect.com/science/article/pii/S0022285206000798>.
[66] R. Marquardt, K. Sagui, J. Zheng, W. Thiel, D. Luckhaus, S. Yurchenko, F. Mariotti, M. Quack, J. Phys. Chem. A 117 (2013) 7502–7522, https://doi.org/10.1021/jp4016728. <http://pubs.acs.org/doi/abs/10.1021/jp4016728>.
[67] S. Albert, K. Keppler Albert, H. Hollenstein, C. Manca Tanner, M. Quack, Fundamentals of rotation – vibration spectra, in: M. Quack, F. Merkt (Eds.), Handbook of High Resolution Spectroscopy, vol. 1, Wiley, Chichester, 2011, pp. 117–173.